Minimal Surfaces and Structures: From Inorganic and Metal Crystals to Cell Membranes and Biopolymers

STEN ANDERSSON,*† S. T. HYDE,‡ KÅRE LARSSON,§ and SVEN LIDIN†

Inorganic Chemistry 2, Chemical Center, University of Lund, Box 124, Lund, Sweden, Department of Applied Mathematics, Institute of Advanced Studies, Australian National University, Box 4, Canberra, Australia, and Department of Food Technology, Chemical Center, University of Lund, Box 124, Lund, Sweden

Contents

I. Introduction

Over the past few years we have explored the use of differential geometry and minimal surfaces in chemistry. We have applied it to describe inorganic or metal structures,[1-3] non-Euclidean saddle polyhedra and nets, phase transitions such as the martensite transformation,[4] the absorption of gases in zeolites,[5] the structures and transformations of lipid bilayers,[6] and the structure of starch[7] and also to derive a model membrane consisting of a lipid bilayer with a regular array of protein units.[8] We have enjoyed an excellent collaboration with H. G. von Schnering and R. Nesper of MPI, Stuttgart,

and their discovery[9,10] that solids have periodic equipotential or zero-potential surfaces, which are identical, or nearly so, with periodic minimal surfaces, is of course very important.

In order to perform these studies it was essential for us to comprehend the mathematics of periodic minimal surfaces. A first and important step was the numerical solution of the Weierstrass equations.[2] Most important of all was the systematic derivation of complex analytic functions $(R(\omega))$ for any minimal surface.[11] A third step is the use of space group stereohedra derived by Bashkirov as free boundaries in obtaining several new intersection-free periodic minimal surfaces.[12] A fourth and equally important step must be the work by Fischer and Koch[13] in describing a method to deduce all group–subgroup pairs of space groups compatible with five new beautiful periodic minimal surfaces without self-intersections. Two of these surfaces seem to be similar[13] to two of those derived by Schnering and Nesper by Ewald calculations. This is not surprising considering that similar symmetry conditions are used by the two groups in their work in finding new surfaces useful in solid-state science.

The basic idea behind this work is that the intrinsic properties of these surfaces in their representation of molecules or structures must provide us with information about the connection between curvature and bonding, or, in other words, how to describe the chemical bond with differential geometry. This will then help us to understand how atoms or ions move in solids and how porous solids such as zeolites, "barrel"-like proteins, and helicoid-shaped molecules such as cellulose, collagen, and starch absorb and/or transform other molecules or catalyze reactions; a structure in its bonding and interaction with molecules follows the metric of its surface.

II. Short History

Early last century the first periodic minimal surface (T) was derived by the French mathematician Gergonne. In 1853 Riemann discovered the D surface, and Schwarz rediscovered these two surfaces and added three new ones, the H, CLP, and P, around 1880.[14] Neovius, a student of Schwarz, realized that the P and D surfaces are related by the Bonnet transformation and used this technique to derive his surface.[15] In the 1960s the American physicist Alan Schoen discovered many new periodic minimal surfaces using soap films with partially free boundaries[16,17] Donnay, Nissen, and

† Inorganic Chemistry 2, Chemical Center, University of Lund.
‡ Department of Applied Mathematics, Institute of Advanced Studies, Australian National University.
§ Department of Food Technology, Chemical Center, University of Lund.

Sten Andersson is since 1983 Professor at the Chemical Center, University of Lund. His thesis (1967) concerned the systematics of structures of inorganic oxides. Currently, his research concerns the understanding of structures in general.

Stephen Hyde obtained his Bachelor's degree in science from the University of Western Australia and Monash University, Melbourne. In 1986 he obtained his doctorate from Monash University, after collaboration with Professor Andersson in Lund. He now works at the Department of Applied Mathematics, Australian National University, Canberra.

Kåre Larsson is since 1975 Professor at the Chemical Center, University of Lund. His thesis (1964) concerned the crystal structure and polymorphism of lipids. Currently, his research concerns the physical chemistry of biomolecules and technical applications.

Sven Lidin is a graduate student at the Department of Inorganic Chemistry 2 in Lund. He received his MSc from the Lund Institute of Technology in 1986.

Pawson recognized the morphology of single calcite crystals in platelets of sea urchins to be that of the P surface.[18] Scriven[19] was the first to suggest periodic minimal surfaces as a model for liquid crystal phases in 1976, and this was developed further by Larsson, Fontell, and Krogh[20] in 1980. The similarity between surfaces and zeolite structures was recognized by Mackay in 1979.[21]

III. Why Minimal Surfaces

In a search for unifying methods of describing complicated crystal solids, B. G. Hyde and one of us put forward a logical and axiomatic theory a few years ago.[21-23] One finding was that complicated structures can be described as built of small units of simple structures or building blocks—the mathematical tool is then obviously *matrix algebra*.[24]

The blocks are always repeated to build a structure via the classical operations: translation, rotation, and reflection.

A good illustration of this is the giant structure of the zeolite paulingite, worked out by Samson and Gordon[25] and described by us as built up of blocks of the much simpler zeolite merlinoit.[26] This is illustrated in Figure 1.

Another important and common way of forming a structure is the interpenetration of two structures, identical[27] or different.[23] When the giant structure of zeolite N[28] was solved by letting parts of two simpler zeolites, sodalite and ZK5, interpenetrate (Figure 2), it was realized that the interface between these two could be described as a periodic non-self-intersecting minimal surface.[29] It was also understood that all structures built via interpenetration can be described by the concept of minimal surfaces.

Whereas the matrix algebra approach is Euclidean, the minimal surface approach is non-Euclidean. The mathematics of the latter is based on the calculus of variations as shown by Lagrange *and* differential geometry. In terms of physics the matrix technique is static to its nature, while *calculus* and differential geometry allow dynamic applications. A soap film spanned between fixed boundaries is an optimal form that of course responds to a minimum of energy. A structure that can be fitted to a minimal surface can be described with *calculus* and is also the *optimal* form.

Differential geometry and calculus of variations proceed in different directions; in differential geometry we study the vicinity of a point on a surface and derive the overall structure from this. In the calculus we deduce local properties from the whole.

IV. Mathematics

For a complete understanding of the usefulness of periodic surfaces in describing solids and its properties, it is neccessary to review the differential geometry needed. Readers unfamiliar with this branch of mathematics may want to consult a textbook on the subject.
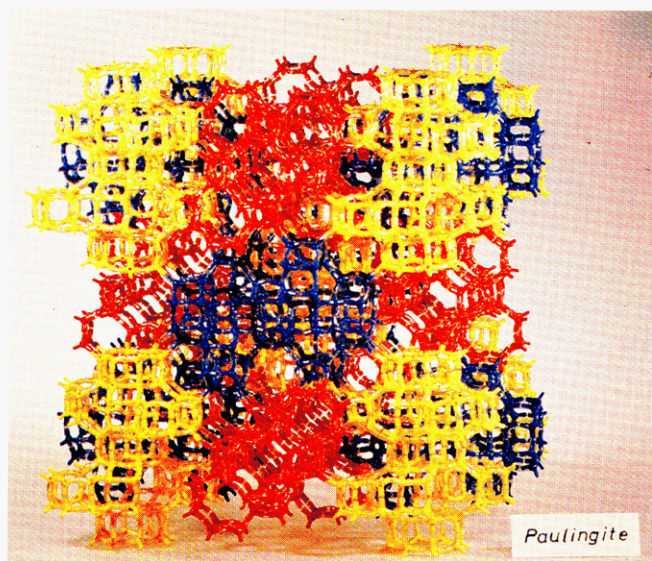
Figure 1. Structure of paulingite.

Figure 2. Structure of zeolite N.

During our work we have found ref 70–72 commendable. A charming and very readable introduction is given by Hildebrandt.[73]

Classically, a surface's equation is written in Monge's form

$$z = F(x,y)$$

For many reasons it is better to use two independent parameters, u^1 and u^2, in a vector equation for the surface (Figure 3):

$$\mathbf{r} = \mathbf{r}(u^1, u^2)$$

By defining the basic tangent vectors $\mathbf{r}_1$ and $\mathbf{r}_2$ we have

$$d\mathbf{r} = \mathbf{r}_1 \, du^1 + \mathbf{r}_2 \, du^2$$

$$\mathbf{r}_1 = d\mathbf{r}/du^1, \qquad \mathbf{r}_2 = d\mathbf{r}/du^2$$

$r_1 r_2$ is the tangent plane to the surface at the point (u^1, u^2). The basic vectors have components g_{ij} such that

$$g_{11} = \mathbf{r}_1 \cdot \mathbf{r}_1 | g_{22} = \mathbf{r}_2 \cdot \mathbf{r}_{21} | g_{12} = \mathbf{r}_1 \mathbf{r}_2$$

g_{ij} is called the metric tensor.

We have then the formula for the element of arc ds, *the first fundamental form.*

$$ds^2 = d\mathbf{r} \cdot d\mathbf{r} = g_{11}(du^1)^2 + 2g_{12} \, du^1 \, du^2 + g_{22}(du^2)^2$$

$$g = \begin{vmatrix} g_{11} & g_{12} \\ g_{12} & g_{22} \end{vmatrix}$$

In the case of orthogonal parametric curves, u^1 and u^2, $g_{12} = 0$, $g = g_{11}g_{22}$, and

$$ds^2 = g_{11}(du^1)^2 + g_{22}(du^2)^2$$

We introduce the important notation

$$b_{ij} = \mathbf{r}_{ij} \cdot \mathbf{n}$$

$\mathbf{n}$ is the normal vector to the surface $\mathbf{r} = \mathbf{r}(u^1, u^2)$. κ is the normal curvature, different in different directions, of a plane curve, formed by the section of the normal plane and the surface.

We have the *second fundamental equation*:

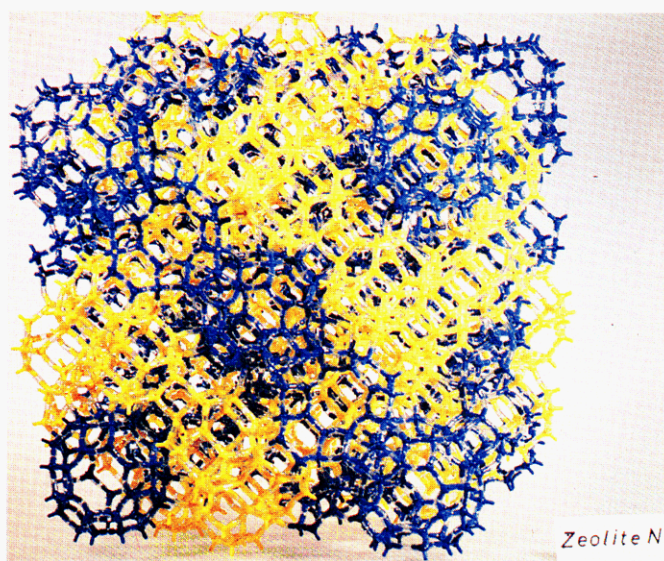$$\kappa \, ds^2 = b_{11}(du^1)^2 + 2b_{12} \, du^1 \, du^2 + b_{22}(du^2)^2$$
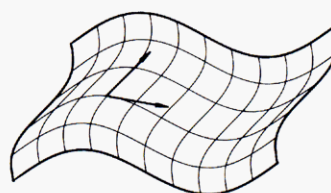

Figure 3. Vector representation of a surface.

In conclusion we say that the first fundamental equation is a measure of the metric of the surface, while the second is a measure of its flatness.

When the normal plane rotates, we obtain maximum values of κ; κ_1 and κ_2. They are then called principal curvatures, and the corresponding curves of intersection are called principal lines of curvature.

The principal curvatures κ_1 and κ_2 have a product and an arithmetic mean known as the *Gaussian curvature K* and the *mean curvature H*

$$\kappa_1 + \kappa_2 = 2H$$

$$\kappa_1 \kappa_2 = K$$

It can be shown that

$$K = \frac{b}{g} = \frac{b_{11}b_{22}}{g_{11}g_{22}}$$

$$2H = \frac{b_{11}}{g_{11}} + \frac{b_{22}}{g_{22}}$$

and the general formula for **K** is

$$\mathbf{K} = -\frac{1}{g^2} \begin{vmatrix} 0 & \dfrac{1}{2}\dfrac{dg_{11}}{du^2} & \dfrac{1}{2}\dfrac{dg_{22}}{du^1} \\ -\dfrac{1}{2}\dfrac{dg_{11}}{du^2} & g_{11} & g_{12} \\ \dfrac{1}{2}\dfrac{dg_{22}}{du^1} & g_{21} & g_{22} \end{vmatrix}$$

and

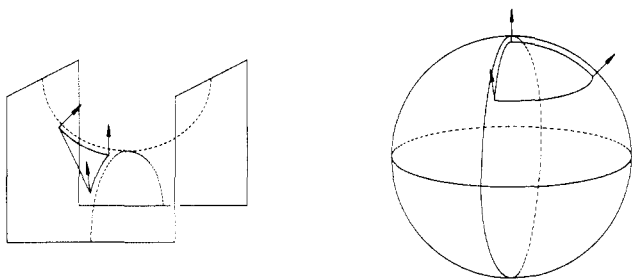$$H = \frac{1}{2}\frac{g_{11}b_{22} - 2g_{12}b_{12} + g_{22}b_{11}}{g}$$
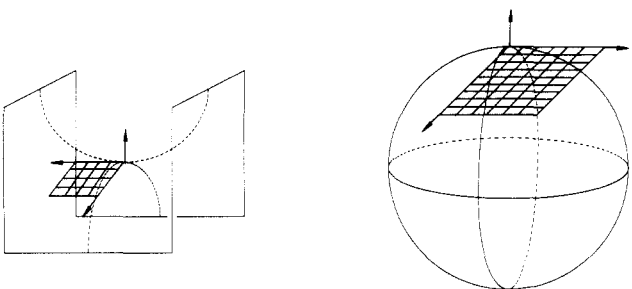
Figure 4. Spherical image of a surface.

Figure 5. Spherical image of a cross-product.

An easier understanding of K is perhaps obtained by spherical or Gaussian mapping. A domain Ω on a surface has a spherical image Ω^*. When those two domains approach a point P (P*), the limit of their ratios is $\mathbf{K}$ (Figure 4).

Similarly the spherical image of tangent vector cross products (tangent vectors to a surface) equals the tangent vector cross product multiplied by $\mathbf{K}$ (Figure 5). A simple relationship also exists for H.

It is of special interest to study how the intrinsic properties behave under mapping, or surface transformations. The most restricted of all mappings is the *isometric*, when the image of an arc equals itself, going from one surface to another. Length and angles are preserved. This means one surface can be transformed into another without tearing or stretching; just bending occurs. During this procedure the Gaussian curvature $\mathbf{K}$ is not changed, and this is called a *Bonnet* transformation.

The *conformal* mapping preserves angles (one example is the stereographic or Mercator projection), while the *isoareal* mapping preserves areas.

Geodesic curvature is a measure of how much a line or curve deviates from being geodesic. Another way of stating this is that a geodesic line of a surface is a curve whose geodesic curvature is zero at every point. A geodesic AB is the shortest path from A to B on the surface.

One of the most important—and simple—formulas in differential geometry in order to characterize a surface in the large is the Gauss–Bonnet formula (Figure 6):

$$\text{mth} \int \int_{\Omega} K \, ds + \int k_g \, ds + \sum \alpha_i = 2\pi$$

K is Gaussian curvature, and K_g is geodesic curvature.

If the domain Ω is bounded by a geodesic polygon, i.e., the contour lines are geodesic lines, then $\int k_g \, ds = 0$, and

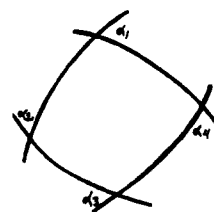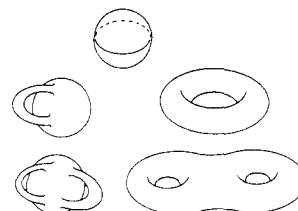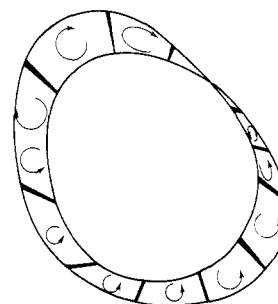$$\int \int_{\Omega} K \, ds + \sum \alpha_i = 2\pi$$

Figure 6. Polygon on a surface with exterior angles α.

Figure 7. Standard orientable topological surfaces: the sphere (genus = 0), the torus ($g = 1$) (with the topologically equivalent one-handled sphere), and the two-handled sphere, with the topologically equivalent "pretzel" surface ($g = 2$).

Figure 8. A Möbius band. One-sided and nonorientable surface.

In particular, for a geodesic triangle with interior angles α, β, and γ we have

$$\alpha + \beta + \gamma - \pi = \int \int_{\Omega} K \, ds$$

In connection with integral curvature it is useful to discuss other properties of a surface genus (g) and Euler–Poincaré's characteristic (χ). We have the relationship

$$\chi = V - e + f$$

where in a domain, with boundaries being curvilinear polygons, v is the number of vertices, e is the number of edges, and f is the number of domains. Furthermore

$$\chi = 2 - 2g; \quad \text{oriented surface}$$

$$\chi = 1 - g; \quad \text{nonoriented surface}$$

and

$$\int \int K \, ds = 2\chi\pi$$

For example, if the genus for a minimal surface is 3 per unit cell, χ is −4 and the integral curvature per unit cell is 8π. Examples of oriented surfaces and their genus are given in Figure 7. The archetypal nonoriented surface ("one-sided" surface) is the Möbius strip (Figure 8).

Often in description of structures with minimal surfaces, atoms sit outside the surface, on parallel surfaces.

If $\mathbf{r} = \mathbf{r}(u^1,u^2)$ is the equation for the surface, its parallel has the equation

$$R = \mathbf{r}(u^1,u^2) + a\mathbf{m}(u^1,u^2)$$

a is the perpendicular distance between the surfaces. Then we have

$\tilde{H}$ (mean curvature for parallel surface) =

$$\frac{H - aK}{1 - 2aH + a^2K}$$

$\tilde{K}$ (Gauss curvature for parallel surface) =

$$\frac{K}{1 - 2aH + a^2K}$$

In the case of a minimal surface, $H = 0$

$$\tilde{H} = -\frac{aK}{1 + a^2K}$$

$$\tilde{K} = \frac{K}{1 + a^2K}$$

and

$$\tilde{H}/\tilde{K} = -a$$

For a surface parallel to a minimal surface, the mean and Gaussian curvatures are proportional. It is also known that the area of the parallel surface is always the smaller.

V. Minimal Surfaces

Surfaces of zero mean curvature are called minimal surfaces:

$$g_{11}b_{22} - 2g_{12}b_{12} + g_{22}b_{11} = 0$$

With orthogonal parametric curves $g_{12} = 0$ and for a minimal surface it is possible to choose u^1 and u^2 so that $g_{11} = g_{22}$ (isothermic coordinates)

$$b_{22} + b_{11} = 0 \text{ or } r_{11} + r_{22} = 0$$

which means that minimal surfaces always can be described with the Laplace equation.

To our knowledge only a few minimal surfaces are simply parametrized and defined by analytic functions in Cartesian space. Some of these are the *catenoid*, the *helicoid*, and the two-dimensional periodic *Scherk surface*. The *catenoid* has the parametric equations

$$x = a \cosh \frac{u^1}{a} \cos u^2$$

$$y = a \cosh \frac{u^1}{a} \sin u^2$$

$$z = u^1$$

and is a surface of revolution, resulting from rotation of the catenary. Its first fundamental form is

$$ds^2 = \cosh^2 \left[\frac{u^1}{a}[(du^1)^2 - a^2(du^2)^2] \right]$$

The *helicoid* is the only minimal surface that is a ruled surface—the surface is covered by straight lines perpendicular to the helical axis which are called rul-
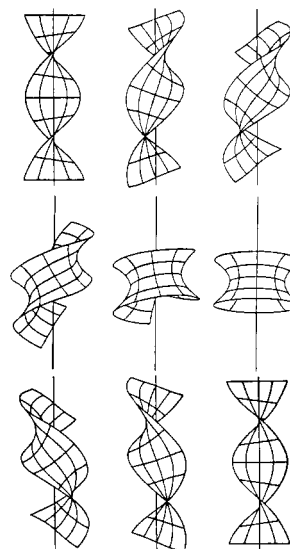

Figure 9. The Bonnet transition linking the helicoid and the catenoid. Note the change in handedness of the helicoid. The curves in the catenoid are plane lines of curvature, which transform under the Bonnet transformation to the straight lines of the helicoid.

ings. The helicoid has the property that its helix curves are asymptotes, and if the helix is circular, these lines are also geodesics. The helicoid is described with the following parametric equations

$$x = u^1 \cos u^2$$

$$y = u^1 \sin u^2$$

$$z = au^2$$

and by its first fundamental form

$$ds^2 = du^2 + (u^2 + a^2) \, dv^2$$

The two surfaces are shown in Figure 9, which also describes their Bonnet transformation (see below).

Infinite minimal surfaces, periodic in three dimensions, cannot be defined by analytic functions in Cartesian space. In order to repeat a surface element periodically throughout space, it must be made finite and the surfaces are described by elliptic integrals, which must be solved numerically. On the other hand, minimal surfaces are the only surfaces other than the sphere whose spherical representation is conformal. This means every complex analytic function can be used to define a minimal surface. It is a fact that the description of infinite periodic minimal surfaces in the complex plane is extremely simple.

A point $P(x,y,z)$ on the surface s is transformed by the normal mapping to a point $P'(x',y',z')$ on the unit sphere given by

$$P'(x',y',z') =$$

$$\left(\frac{dF}{dx}, \frac{dF}{dy}, \frac{dF}{dz} \right) \bigg/ \left(\left(\frac{dF}{dx}\right)^2 + \left(\frac{dF}{dy}\right)^2 + \left(\frac{dF}{dz}\right)^2 \right)^{1/2}$$

which is transformed via the stereographic projection to the point $P''(x'',y'')$:

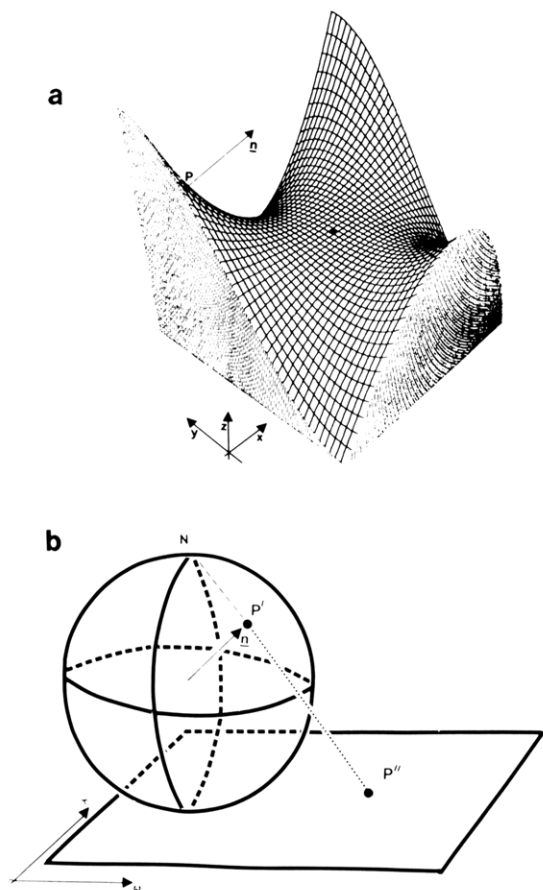$$(x'',y'') \equiv (\sigma,\tau) = \left(\frac{x'}{1 - z'}, \frac{y'}{1 - z'} \right)$$

Figure 10. (a) An arbitrary surface, showing the normal vector **n** at a point P. (b) Procedure for mapping a minimal surface onto the complex plane used for the Weierstrass representation. The normal vector is used to map the original point P onto a point on the unit sphere, centered at P, to give the point P′, which is then mapped by stereographic projection onto the complex plane.

The surface s can in the complex plane be simply described by an analytic complex function, $R(\omega)$, where

$$\omega = \sigma + i\tau \quad (i \text{ is the complex constant})$$

The conformal mapping is shown in Figure 10.

Karl Weierstrass found that the Cartesian dimensions of a point $P(x,y,z)$ on a minimal surface are related to the coordinates of its mapped point $P''(\sigma,\tau)$ by

$$x = \text{Re} \int (1 - \omega^2)R(\omega) \; d\omega$$

$$y = -\text{Im} \int (1 + \omega^2)R(\omega) \; d\omega$$

$$z = \text{Re} \int 2\omega R(\omega) \; d\omega$$

where Re and Im denote the real and imaginary parts of the complex integral. The Weierstrass polynomial, $R(\omega)$, determines all intrinsic geometric parameters of the surface. At a point ω, the metric is given by

$$ds^2 = (1 + \omega^2)|R(\omega)||d\omega|$$

This is the first fundamental form and can also be described with the fundamental metric tensor g_{ij}:

$$ds^2 = g_{11} \; d\sigma^2 + (g_{12} + g_{21}) \; d\sigma \; d\tau + g_{21} \; d\tau^2$$

which gives

$$g_{11} = g_{22} = (1 + |\omega|^2)^2|R(\omega)|^2; \; g_{12} = g_{21} = 0$$

and the Gaussian curvature becomes

$$K = -4(1 + |\omega|^2)^{-4}|R(\omega)|^{-2}$$

Similarly elements b_{ij} of the second fundamental form can be obtained:

$$b_{11} = -2 \; \text{Re} \; [R(\omega)] = b_{22}$$

VI. Transformations of Surfaces

1. The Bonnet Transformation

Schwarz described the D, P, CLP, H, and T surfaces. Schoen discovered the body-centered cubic minimal surface called the gyroid, G. D, P, and G are related by a transformation named after Bonnet, who described it 1853. Surfaces related by a Bonnet mapping are called associate. A Bonnet-transformed minimal surface has real space coordinates

$$x = \text{Re} \int e^{i\theta}(1 - \omega^2)R(\omega) \; d\omega$$

$$y = -\text{Im} \int e^{i\theta}(1 + \omega^2)R(\omega) \; d\omega$$

$$z = \text{Re} \int e^{i\theta}(2\omega)R(\omega) \; d\omega$$

where θ is called the association parameter. If $S(\theta)$ denotes an associate surface, it can be shown that

$$g_{11}S(\theta) = g_{22}S(\theta) = (1 + \omega^2)^2|e^{i\theta}R(\omega)|^2 =$$
$$(1 + \omega^2)^2|R(\omega)|^2 = g_{11}(S) = g_{22}(S)$$

Also

$$b_{11}S(\theta) = -2 \; \text{Re} \; [e^{i\theta}R(\omega)] = -2 \cos \theta \; \text{Re} \; [R(\omega)] =$$
$$\cos \theta b_{11}(S)$$

All associate surfaces have the same metrics. It is also easy to show that all associate surfaces to minimal surfaces are themselves minimal surfaces.

Since all associate surfaces have the same metrics, all lengths are preserved during the transformation, which is isometric, and also conformal. The Bonnet transformation thus only bends the surface, without stretching. A good example of this is shown in Figure 9, where the catenoid is Bonnet transformed via a number of associate surfaces (most of them would be self-intersecting) to the helicoid.

At corresponding points on the family of associate surfaces, the Gaussian curvature is unchanged.

Since

$$e^{i(\theta+\pi)} = -e^{i\theta}$$

$$(x,y,z)(S_\theta) = -(x,y,z)S_{\theta+\pi}$$

which means that surfaces with association parameters differing by π are related by center of symmetry.

Similarly, since

$$\text{Re} \; (e^{-i\theta}) = \text{Re} \; (e^{i\theta})$$

and

$$\text{Im} \; (e^{-i\theta}) = -\text{Im} \; (e^{i\theta})$$

$$x(S_{-\theta}) = x(S_\theta)$$

$$y(S_{-\theta}) = -y(S_\theta)$$

$$z(S_{-\theta}) = z(S_\theta)$$

Surfaces with association parameters of opposite sign are related to each other by reflection in the x,z plane. Consequently, chiral minimal surfaces are related to their enantiomorph through the Bonnet transformation. This is shown in Figure 9, where the handedness of the helicoid is changed between association parameters of $-\pi/2$ and $+\pi/2$.

Surfaces with association parameters differing by $\pi/2$ are known as adjoint surfaces, since they are described by adjoint (conjugate) complex functions.

Corresponding points on Bonnet-related surfaces trace out point trajectories (plane curves) in real space, which are ellipses centered on the origin of the coordinate system chosen.

Coordinates (x,y,z) of a surface S are related to the coordinates (x',y',z') of the associated surface and the coordinates (x^*,y^*,z^*) of the adjoint surface by

$$(x',y',z') = (x,y,z) \cos\theta + (x^*,y^*,z^*) \sin\theta$$

If the Bonnet transformation is applied to periodic minimal surfaces, associate surfaces need not be periodic, but if they are, certain symmetry properties need to be described. If a minimal surface is periodic, its *adjoint* is also periodic.[30] All geodesics remain geodesic under the Bonnet transformation, while straight lines transform so that they become plane lines of curvature in the adjoint surface and vice versa.

2. The Goursat Transformation

A second, more general, minimal surface transformation was explored by Goursat.[31] A family of minimal surfaces is formed by varying a parameter k in the Weierstrass parametrization:

$$x = \operatorname{Re} \int (k - \omega^2) \frac{1}{k} R(\omega) \, d\omega$$

$$y = -\operatorname{Im} \int (k + \omega^2) \frac{1}{k} R(\omega) \, d\omega$$

$$z = \operatorname{Re} \int 2\omega R(\omega) \, d\omega$$

The metric for the derived surface is

$$ds^2(S_k) = \left(k + \frac{\omega^2}{k} \right) |R(\omega)| |d\omega|$$

Thus the Goursat transformation stretches the surface, as well as bending it. Nevertheless, the transformation is conformal, preserving angles. The Gaussian curvature for the derived surface is

$$k(S_k) = -4 \left[k + \frac{\omega^2}{k} \right]^{-4} |R(\omega)|^{-2}$$

In real space, the derived surface coordinates (x',y',z') are related to the Bonnet-related surface coordinates on the original surface and its adjoint (x,y,z) by

$$x' = x \left(\frac{1 + k^2}{2k} \right) + y^* \left(\frac{1 - k^2}{2k} \right)$$

$$y' = y \left(\frac{1 + k^2}{2k} \right) + x^* \left(\frac{k^2 - 1}{2k} \right)$$
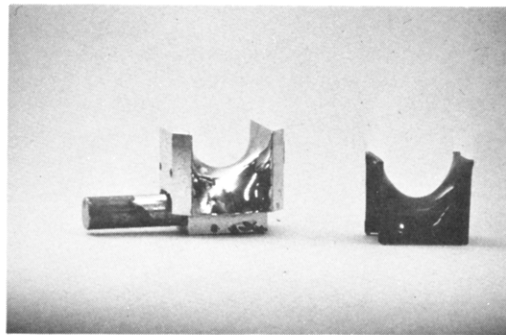
$$z' = z$$

Figure 11. A mold of brass for production of plastic units for the T surface.

Besides that the transformation is conformal and angles are preserved, lines of curvature and asymptotic lines are also preserved on all derived surfaces. Planar lines of curvature remain planar lines of curvature (this does not imply that mirror planes are necessarily preserved). Asymptotic lines (straight lines) lying on a minimal surface, which are axes of skew symmetry in the original surface, remain straight lines. Helicoids remain helicoids.

VII. Weierstrass Polynomials and the Construction of Surfaces

The Schwarz surfaces, P, D, T, H, and CLP, are easily built by using brass forms as molds to produce plastic units as shown in Figure 11. The brass forms were machined after wire models dipped into soap solutions. The wire models were for the P surface the six edges of an octahedron, for the D surface the four edges of a tetrahedron, and for the T surface eight edges of a cube. For the CLP surface, the boundaries form a part of a trigonal prism. For the H surface, a wire triangle, resting on a glass plate and in soap, was lifted up, so that the triangle surface was kept parallel with the plate. Using the symmetry property of minimal surfaces of straight lines being a twofold axis, larger units of these surfaces were built and are shown in Figure 12. Periodic minimal surfaces are always composed of saddles, monkey saddles, and helicoids. A typical saddle is the tetrahedral unit, and six of these form a monkey saddle (Figure 13). The presence of monkey saddles makes the surface periodic. A helicoid is formed by tetrahedral units joined by edges. Notice that a helicoid from a periodic minimal surface is not circular and cannot be ruled like the analytical helicoid described in the beginning of this article.

The family of associate surfaces related to the P and D surfaces is described by Schwarz in the complex plane by the function

$$R(\omega) = \frac{1}{(1 - 14\omega^4 + \omega^8)^{1/2}}$$

A simple "Flächenstück" (surface element) of the D surface, the tetrahedral unit, may be represented in the complex plane by the "Kreisbogenviereck" (circular tetragon), shown in Figure 14. The singularities $((3^{1/2} - 1)/2^{1/2}, 0)$ etc. correspond to the singularities for $R(\omega)$ as defined above. Corresponding coordinates for the adjoint P and D surfaces were determined numerically by computing the elliptic integrals by substituting
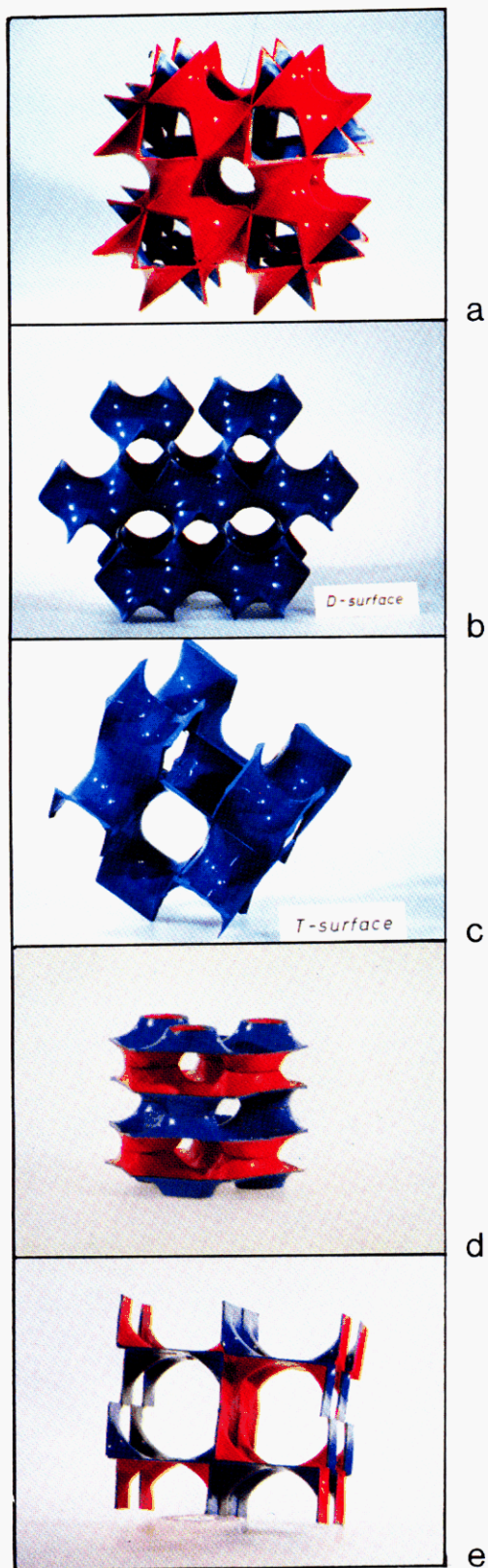
a

b

c

d

e

Figure 12. P (a), D (b), T (c), H (d), and CLP (e) minimal surfaces.

Schwarz's expression for $R(\omega)$ into the Weierstrass equations.[3] Graphic representations of selected parts of these surfaces are shown in Figure 15.

Using Schoen's angle of association of 38.015° to obtain the Bonnet-related gyroid surface, boundary coordinates for a single gyroid "Flächenstück" were
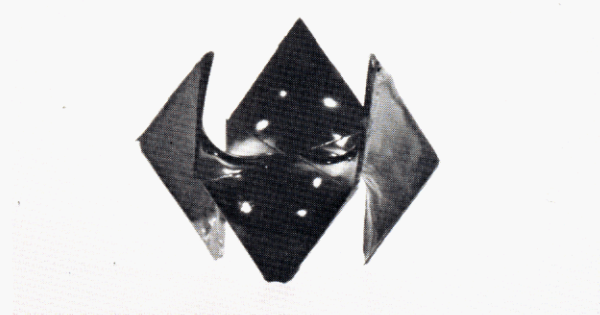

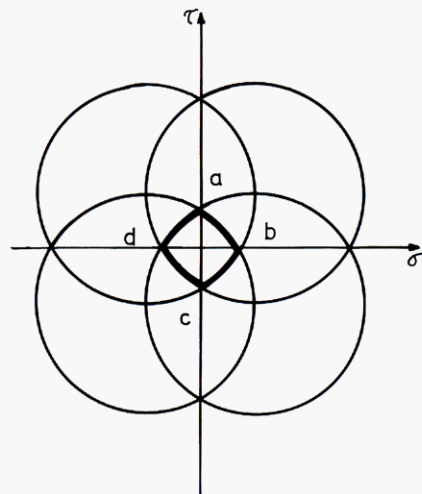**Figure 13.** A monkey saddle consisting of six tetrahedral saddles, the D surface.

Figure 14. Complex plane representation of the tetrahedral unit of the D surface, and associate surfaces (in particular, the gyroid and P surface). Each edge of the "Kreisbogenviereck" abcd is an arc of a circle of radius $2^{1/2}$ centered at $(\pm1/2^{1/2}, \pm i/2^{1/2})$. The points a, b, c, and d are singularities and have coordinates $(\pm(3^{1/2} - 1)/2^{1/2})$ ● $i(3^{1/2} - 1)/2^{1/2}$.
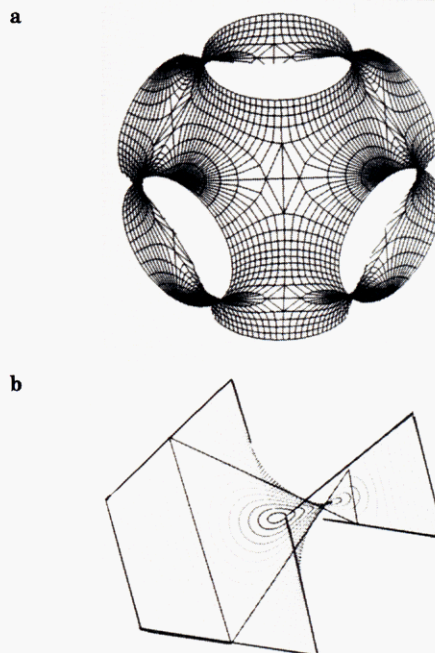
a

b

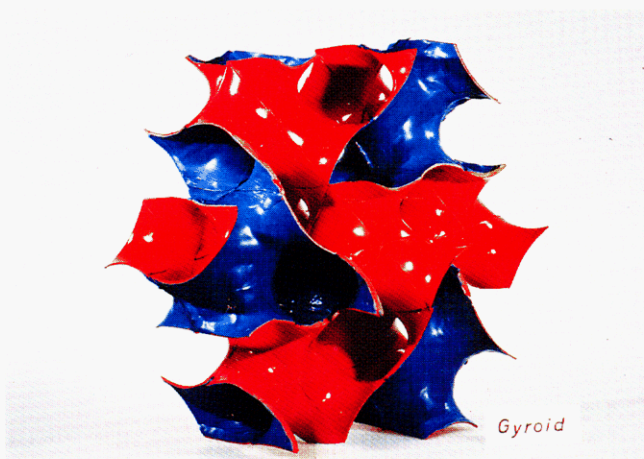**Figure 15.** Graphic representation of the P surface (a) and the D surface (b).
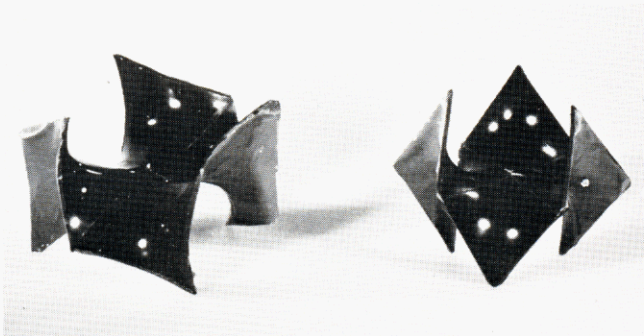
Figure 16. The gyroid surface.

Figure 17. The Bonnet transformation F → G.

Figure 18. Boundaries for D, gyroid, and P surfaces, from top to bottom.

calculated by using the data from D and P. A typical gyroid boundary coordinate, x_i, is given by

$$x_i = x_i(D) \cos (38.015°) + x_i(P) \sin (38.015°)$$

where $x_i(D)$ and $x_i(P)$ are corresponding D and P surface boundary coordinates. A brass form was machined with these boundaries and used as a mold to produce plastic units to build the gyroid shown in Figure 16.

The Bonnet transformation of D → G obtained just by bending is demonstrated in Figure 17, where the monkey saddles are compared. Note that each edge of the gyroid is a skew curve. The axes and surface boundaries for the three surfaces are shown in Figure 18.

VIII. Derivation of Weierstrass Polynomials for the Schwarz T, CLP, and H Surfaces

The Weierstrass polynomial for the family of associate surfaces related to the P and D surfaces is

$$R(\omega) = \frac{1}{(1 - 14\omega^4 + \omega^8)^{1/2}}$$

This polynomial may be written as

$$R(\omega) \frac{1}{\prod_{i=1}^{8}(\omega - \omega_i)^{1/b}}$$

where the $\prod$ sign denotes the product of the eight component factors. $R(\omega)$ can be considered as a multisheeted Rieman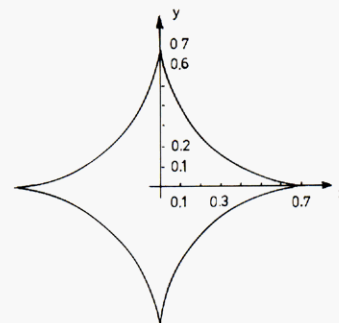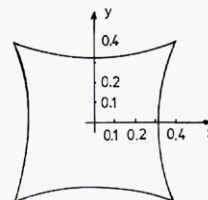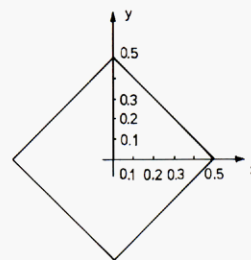n surface. The sheets are connected at branch points, which are analogous to the spherical images of the monkey saddles.

The expression above indicates that the polynomial contains eight isolated singularities corresponding to eight monkey saddles in the spherical image. These eight singularities at ω_i correspond to eight normal vectors at flat points and are the vertices of a cube in the Gauss map.

$$\Delta = |\chi/2|$$

The exponent b_i is determined from the local topology of the minimal surface.[11a]

This suggests a natural generalization to other IPMS, as discussed below. Complex coordinates for flat points are determined via a Gauss map, and the product polynomial $(\omega - \omega_i)$ is then raised to the inverse degree of the Gauss map.

The Gauss maps and complex coordinates were determined for the CLP and T surfaces.[11b] Their common Weierstrass function was found to be

$$(\omega^8 + \Psi\omega^4 + 1)^{-1/2}$$

where Ψ is a parameter determining the nature of the surface: $0 \leq \Psi < -2$, the CLP surface; $\Psi = 2$, the Scherk surface or an associate; $\Psi < -2$, the T surface, with $\Psi = -14$ giving the D surface. The D surface is thus a special case of the tetragonal T surface. The Gauss maps for the CLP and T surface are shown in Figure 19. The complete surfaces are shown in Figure 20, where also the relationships between T and F are clearly revealed. This technique was used to establish the Weierstrass polynomial for the H surface as well.[69]
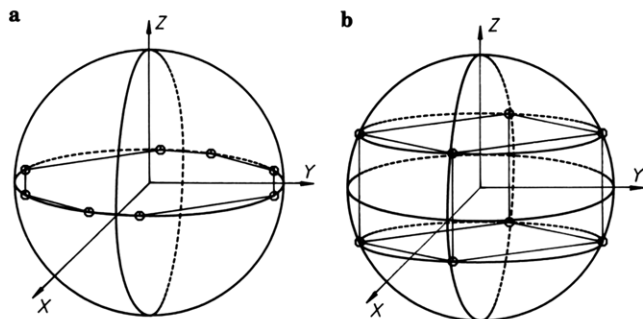
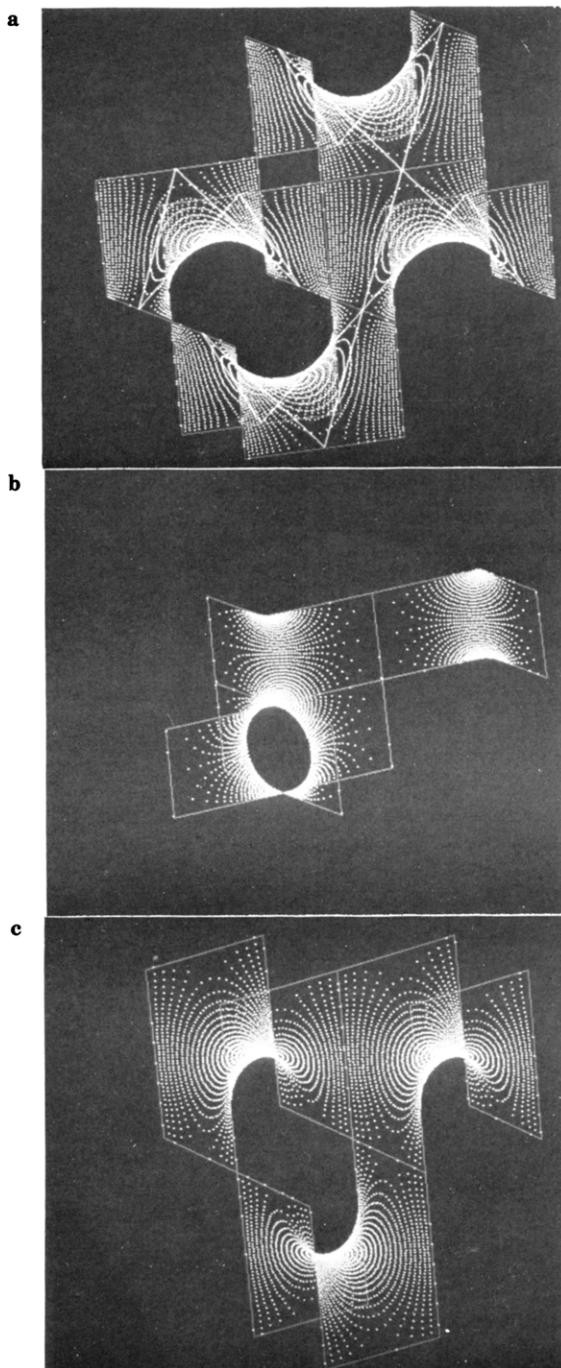**Figure 19.** Gauss maps for the CLP (a) and T (b) surfaces.

Figure 20. Graphic representation of the D (a), CLP (b), and T (c) surfaces revealing their intimate relationships.

IX. Bashkirov Stereohedra and Minimal Surfaces

The handful of classically known translationally ordered minimal surfaces (IPMS) are formed by adjoining identical surface elements bounded by closed skew polygons consisting of straight edges. Smoothness of the surface across the edges is enforced by twofold rotational symmetry about each edge.

The symmetry condition severely constrains the geometry of suitable bounding polygons for IPMS. For example, all vertex angles of the polygon must be integral factors of 360°. Polygonal edge lengths are likewise constrained. Characterization of suitable polygons is possible, based on edges of certain polyhedra known as "kaleidoscopic cells". Any closed circuit consisting of edges of kaleidoscopic cells which are twofold axes (or multiples thereof) of the space-filling arrangement of cells forms a suitable straight-line boundary.

While this criterion guarantees translationally periodic minimal surfaces, most examples derived by this procedure are self-intersecting and nonorientable. More seriously, examples of IPMS without straight lines were discovered by Alan Schoen,[16] so we cannot hope to find all IPMS using linear boundaries. The identification of new IPMS is considerably eased by using free boundaries, consisting of faces of closed cells, rather than fixed edge boundaries.

In order to generate periodic surfaces we choose cells that are asymmetric units of three-dimensional space groups. These cells are equivalent to Coxeter's plane-faced kaleidoscopic cells for reflection groups[40] which were used qualitatively by Schoen to derive IPMS.[16,41] Just as straight boundaries for minimal surfaces induce twofold rotational symmetry in the resulting IPMS, planar boundaries result in reflection symmetry in the boundary plane. This is why kaleidoscopic cells form suitable boundaries for surfaces exhibiting reflection symmetry: the requisite mirror symmetry about each face is ensured by using planar faces.

Conventional asymmetric units of space groups ("stereohedra") are always plane-faced. All minimal surfaces bounded by these cells contain mirror planes lying in cell faces, irrespective of whether the space group defined by the stereohedron contains reflection symmetry planes. In order to ensure that the symmetry of the resulting minimal surface is equivalent to that of the stereohedral honeycomb, all faces and edges must be arbitrarily curved, except where they define mirror planes and twofold rotational axes, respectively. These conditions are met by the stereohedra defined by Bashkirov,[42] who claims that such cells exist for all 230 three-dimensional space groups. In order to generate periodic minimal surfaces of arbitrary symmetry, we therefore derive minimal surfaces bounded by the Bashkirov stereohedron which characterizes the space group of requisite symmetry.

In general, the boundary problem imposed by Bashkirov stereohedra is difficult to solve—heuristics and soap films have had to suffice. A useful necessary condition on appropriate solutions was established by Smyth.[43] The trace of the surface along the faces of the cell must be "balanced", so that the sum of the boundary tangent vectors around the cell faces vanishes.

This constraint is sufficient to determine approximate boundary traces for minimal surface solutions. The exact geometry of boundary traces can then be calculated by using the Weierstrass equations. The surface normal vectors at flat points of the surface (ω_i) fix the poles of the Weierstrass function, as for the P, gyroid, and F surfaces described earlier in this article. The winding number of the Gauss map of the surface around flat points is equal to the inverse of the exponent of the product polynomial (b_i), giving a Weierstrass function

$$R(\omega) = \xi \prod_{i=1}^{n} (\omega - \omega_i)^{-1/b_i}$$

for the n distinct normal vectors in the IPMS. ξ denotes a constant which when totally real determines the lattice parameter of the IPMS. If ξ is imaginary, a family of associate minimal surfaces is generated as its argument is varied. Although associate surfaces are invariably not translationally periodic, the Weierstrass functions constructed from surfaces bounded by Bashkirov stereohedra guarantee IPMS for totally real and totally imaginary values of ξ. It is trivial to ensure that IPMS formed from stereohedral boundaries are free of self-intersections. Since the cells form a tessellation of space, if the surface element bounded by a single stereohedron is free of self-intersections, so is the complete IPMS.

Since all minimal surfaces bounded by a single Bashkirov stereohedron belong to the same space group, many IPMS exist for each space group. Different IPMS of the same symmetry are distinguished by their topology, which is related to the labyrinth net, which defines the tunnel networks on either side of the surface.

The topology of IPMS is most conveniently characterized by the topology of a "compactified" unit cell of the surface, which is formed by "gluing" points on the surface which are related to each other by a lattice vector of the Bravais lattice which describes the translational symmetry of the surface. A unit cell is formed by clustering stereohedra to form a parallelohedron, a procedure which is dependent only on the symmetry.

The IPMS unit cell bounded by a parallelohedron contains tunnels directed toward vertices, edges, and faces of the parallelohedron. If t_0, t_1, and t_2 denote the number of tunnels directed toward vertices, edges, and faces, respectively, and the dihedral angle of the edges containing tunnels is $2\pi/\alpha$, while the dihedral angles of the three edges meeting at the vertices containing tunnels are $2\pi/\beta$, $2\pi/\gamma$, and $2\pi/\delta$, the genus of the IPMS per unit cell is given by

$$g =$$
$$g_c + \frac{t_2}{2} + \frac{\alpha - 1}{\alpha} t_1 + \left\{ \frac{\beta - 1}{\beta} + \frac{\gamma - 1}{\gamma} + \frac{\delta - 1}{\delta} - \frac{1}{2} \right\} \frac{t_0}{2}$$

where g_c is the genus of the closed surface formed by capping all tunnels of a single unit cell.

For example, the Bashkirov stereohedron for the space group $Pm3m$ is one of Coxeter's kaleidoscopic cells, the quadrirectangular tetrahedron. All faces are planar, corresponding to mirror planes of the space group. A simple balanced boundary around the faces of this cell is that shown in Figure 21.[40] The parallelohedron for this space group consists of 48 ster-
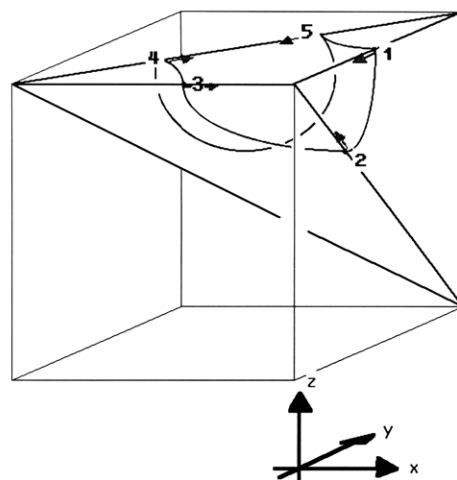

Figure 21. A balanced curve which bounds a minimal surface bounded by a quadrilateral tetrahedron (edges shown as dark lines). The surface normal vectors at boundary vertices (1, 2, 3, 4, 5) are indicated by arrows. This boundary curve is a part of Schoen's O,C–TO minimal surface of space group $Pm3m$.
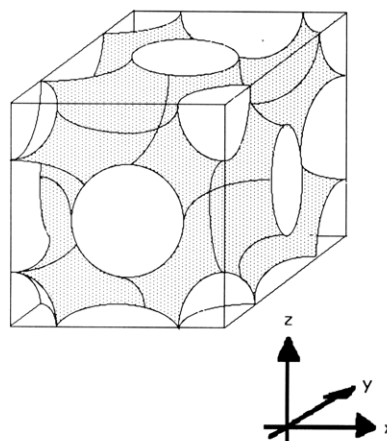

Figure 22. A unit cell of the O,C–TO surface, bounded by a cube.

eohedra, combined to form a cube, giving a unit cell of the IPMS, as shown in Figure 22. This cell contains six face–directed and eight vertex-directed tunnels, with all dihedral angles equal to $\pi/2$. Capping all tunnels results in a closed cell free of handles, so that g_c in the preceeding equation is equal to zero, the genus of a sphere. Hence the genus per unit cell of this IPMS (christened by Schoen the O,C–TO surface) is

$$g = 0 + \frac{6}{2} + 0 + \left\{ \frac{3}{4} + \frac{3}{4} + \frac{3}{4} - \frac{1}{2} \right\} \frac{8}{2} = 10$$

The two labyrinth nets for the O,C–TO surface are different, since the surface lacks straight lines (which would result in equivalent labyrinth nets by twofold rotational symmetry). An alternative description of the O,C–TO surface unit cell is shown in Figure 23 for which the second labyrinth net is centered within the parallelohedron. This net also gives a genus per unit cell of 10 for the O,C–TO surface.

This example illustrates an important property of IPMS. In many cases the two labyrinth nets, and indeed the labyrinth volumes, need not be equivalent. However, the labyrinth nets on either side of the surface are necessarily *topologically equivalent*. In order to be able to separate a structure by a periodic minimal
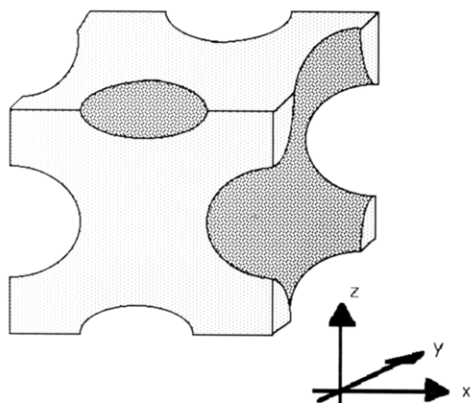
Figure 23. An alternative unit cell of the O,C–TO surface.

Figure 24. The pair of straight edged saddle polyhedra formed by doubly rotating a fundamental linear circuit of the P surface. Those saddle polyhedra together fill space.

Figure 25. Open packings of the saddle polyhedra shown in Figure 24: (a) sharing of P faces results in an open packing bounded by the Neovius surface; (b) sharing of Neovius faces to form the P-surface space filling.

Figure 26. The L saddle polyhedron formed by doubly rotating a linear circuit of the P surface.

surface, the two substructures occupying each labyrinth must be topologically equivalent. If they are not, an open connected partition between the substructures is impossible. This topological equivalence is most simply defined by the condition of "maximal interpenetration" between the two substructural networks (to borrow Wells' concept).[44] In short, any loop of one substructure must enclose a link of the other.

Periodic minimal surfaces are equally well described by "skeletal nets" lying on the surface. Two natural skeletal nets arise, asymptotic nets of vanishing normal curvature and nets of lines of curvature of maximal normal curvature. These nets both form orthogonal grids of arbitrary density everywhere on the IPMS (bar flat points); they are rotated by 45° with respect to each other. IPMS may be characterized by subsets of these nets, consisting of all straight lines on the surface (linear skeletal nets) and all plane lines of curvature (curved skeletal nets). The smallest circuits of linear skeletal nets consist of the linear boundaries derived from kaleidoscopic edges and the infinite nets are generated by successive twofold rotations about each edge. Curved skeletal nets are formed from the boundary trace about plane-faced Bashkirov stereohedra by repeated reflection in the faces of the stereohedral honeycomb. For IPMS lacking both straight lines and plane lines of curvature, curved skeletal nets are given by the boundary trace of the IPMS in the honeycomb of curved stereohedral faces.

These skeletal nets furnish useful descriptions of crystal structures, where the atoms lie in the surface, as described below. This observation is at present largely phenomenological, although work by Greenspan suggests the significance of these surfaces. Arrays of charges, subject to Lennard-Jones type interactions, appear to be most stable when the array tessellates a minimal surface.[45] If this result is indeed general, the apparent crystallization of many structures on IPMS is a necessary consequence of electrostatic interactions.

Skeletal nets on IPMS can also be used to generate space-filling arrays of polyhedra whose faces are minimal surfaces, denoted by Pearce "saddle polyhedra".[46] Any circuit in the net forms the framework for saddle polyhedra by doubly rotating the circuit about an edge, so that every second rotated circuit only forms edges of the polyhedron. By choosing different edges, different saddle polyhedra are often formed, which together fill space. For example, the smallest linear circuit of the P-surface linear skeletal net forms a pair of saddle
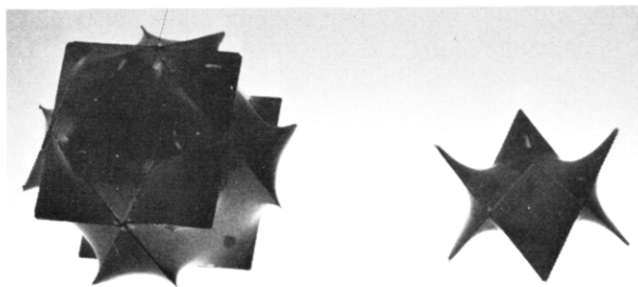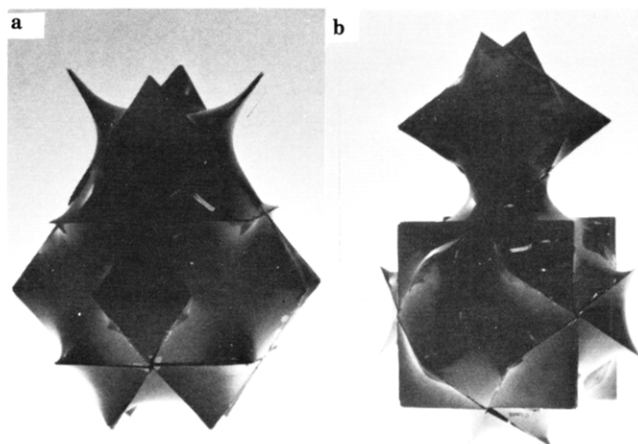
polyhedra, which together fill space (Figure 24). The polyhedra contain skew octagonal faces, which belong to the celebrated Neovius surface[15] in addition to the faces belonging to the P surface. Open packings of these saddle polyhedra form the P and Neovius surfaces, by face sharing of the Neovius and P-surface faces, respectively (Figure 25). These surfaces share the same linear skeletal net and both exhibit $Im3m$ symmetry.

A larger circuit excised from the P-surface linear skeletal net consists of a skew equilateral hexagon, which forms a closed circuit of edges about a regular octahedron. Double rotation of this circuit forms the skeleton of a single-saddle polyhedron, which is space filling (Figure 26). The second face in this cell belongs to the D surface, illustrating the group–subgroup relation between the two surfaces.

Classes of space-filling saddle polyhedra can be formed by doubly rotating successively larger closed

circuits belonging to linear skeletal nets. Resulting faces belong to IPMS whose symmetry is subgroups of the space group of the surface defined by the linear skeletal net, since they contain common symmetry axes.

X. Curvature and Absorption Forces

We proposed early in this project that solids have intrinsic curvature and that it should be possible to describe the chemical bond with differential geometry.[1] For a long time it has been well-known that the porous zeolites absorb gases according to the diameter of the opening of the pores, or the ring size. Typical ring structures contain 6, 8, 10, or 12 SiO_4 tetrahedra. Recently, we managed to relate absorption force and Gaussian curvature for two hydrophobic zeolites, the faujasite structure with 12 rings and the silicalite structure with 10 rings.[32] This was done by using the equation for motion of a particle on a space curve:

$$\mathbf{a} = \frac{dv}{dt}\mathbf{T} + v^2\kappa\mathbf{N}$$

where **a** is the acceleration vector, v is the speed, **T** and **N** are the tangent and normal vectors, and κ is the curvature. If the particle moves on a minimal surface along a principal line of curvature, the total van der Waals force lines are orthogonal to the motion, which is curvilinear. This means speed is constant:

$$|a| = v^2\kappa$$

κ is now $= -K^{1/2}$, where K is the Gaussian curvature. For organic molecules such as the olefins, it is well-known that van der Waals forces are proportional to the number of CH_2 groups; the organization of atoms on a surface gives rise to an electrostatic field that interacts with neighboring molecules. The intrinsic force a molecule feels is set to be proportional to the number of bonding electrons per molecule, N.

$$F = v^2N(-K^{1/2})$$

However, molecules feel forces from *surface elements*, and to describe this we simply use average Gaussian curvature, which we define

$$K_{av} = \int\int K\,ds \text{ per surface unit}$$

where ds is a surface element. The integral curvature measures the intrinsic difference between a region of the surface and a region of the plane, or in simpler terms how much curvature a region of a surface contains (based on the convention that a plane has zero curvature).

$$F = \text{const} \times NK_{av}$$

As shown above $\int\int K\,ds$ is extremely simple to calculate. For a tetrahedral saddle it is $-2/3\pi$, and if the surface area is calculated for such a saddle by numerical integration of the Weierstrass equations, for a hydrophobic faujasite structure of $a = 24.30$, its K_{av} is equal to -0.0444 Å^{-2}. The equation was now tested by using accurate absorption heats of hydrocarbons,[33] and its constant was determined. We have no minimal surface yet for the silicalite structure, but again using accurate heats of absorption,[33] its K_{av} was determined to -0.072 Å^{-2}. The final relationship between heats of absorption,
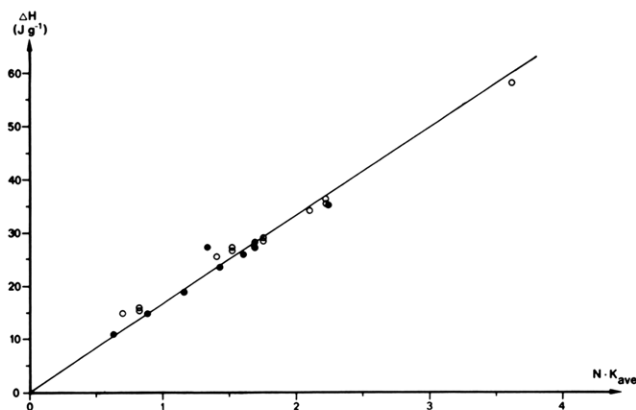

Figure 27. Relationship between heats of absorption for various hydrcarbons, number of bonding electrons (N), and curvature for silicalite and faujasite.
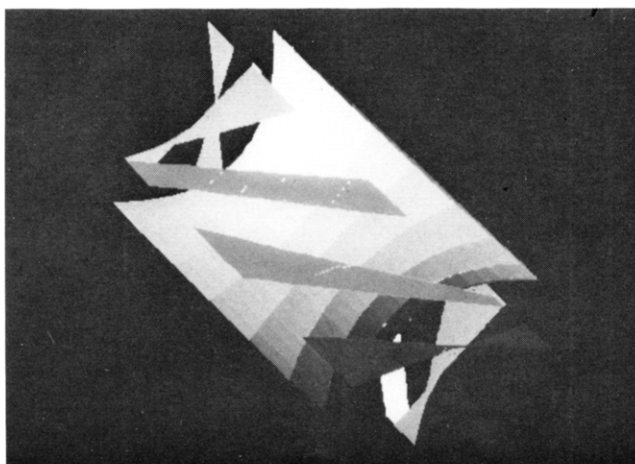

Figure 28. Catenoid description of an α/β "barrel" with its eight strands.

number of bonding electrons, and curvature for these two structures is shown in Figure 27.[32]

It is now interesting to apply these results on other structures which have curvature. Many protein structures are characterized by a so-called "barrel" arrangement; in this arrangement, smaller molecules can enter and undergo catalytic reactions. The "barrel" is formed by eight so-called β strands,[34] which in fact are organized in a catenoid ("bottleneck") arrangement. This is indicated in Figure 28. With the results obtained above we can now estimate the forces that pull smaller molecules through the giant "barrel" molecule and make them pick up heat to react or transform.[33b] Four tetrahedral saddles forming a helicoid in the D surface transform via a Bonnet transformation into a catenoid arrangement of the P surface. The integral curvature of this unit is $-8/3\pi$. If a tetrahedral edge is estimated to be 15–20 Å, K_{av} for a "barrel" is ~0.01 Å^{-2}. This is naturally much lower than the K_{av} derived for the zeolites, but on the other hand the nature of the forces of interaction is different and intrinsic heats high enough to be responsible for reactions are easily developed according to the equation above.

Such β strands also organize themselves into "twisted sheets", which in fact are helicoids, in another group of proteins or enzymes. Again reactions are explained by curvature and absorption.[33b]

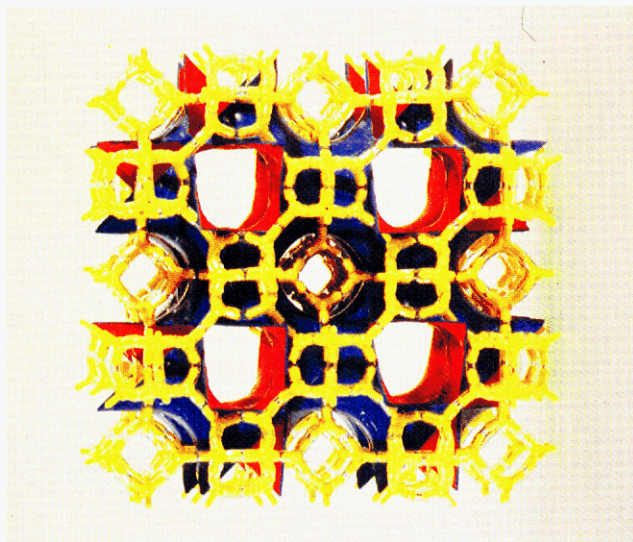Cellulose, collagen, and starch have all-helicoid structures which explain their behavior as adsorbents.

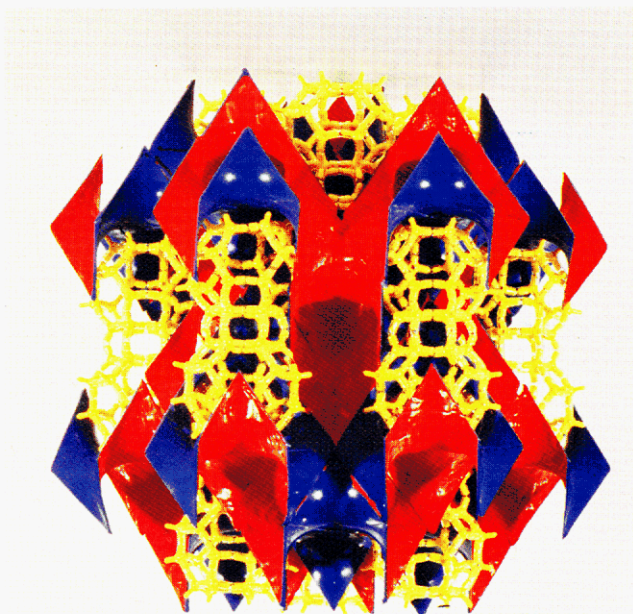**Figure 29.** Linde A zeolite structure and the P surface.

Figure 30. Faujasite zeolite structure and the F surface.

XI. Periodic Minimal Surfaces and Crystal Structures

In Figures 29 and 30 it is shown how the well-known Linde A and faujasite structures fit to one side of the P and D surfaces. Similarly, we have shown how the diamond, cristobalite, cubic ice, and ice VII fit to the D surface (Figure 31). We also described the cubic Na_xWO_3 (a metal conductor) with the P surface, with Na atoms on one side of the surface and WO_6 octahedra on the other. The conducting electrons were suggested to move on geodesics of the surface.[1] This now has support from a recent accurate calculation of the structure of Si.[35] Christensen's charge density plot on the (110) section reveals on equielectron density surface, which, as pointed out to us by von Schnering and Nesper of MPI, Stuttgart, follows the geometry of the D surface. The sodalite structure is noninterpenetrating and its atoms sit on the P or D surfaces (adjoint) (Figure 32a). The analcime structure is also nonin-
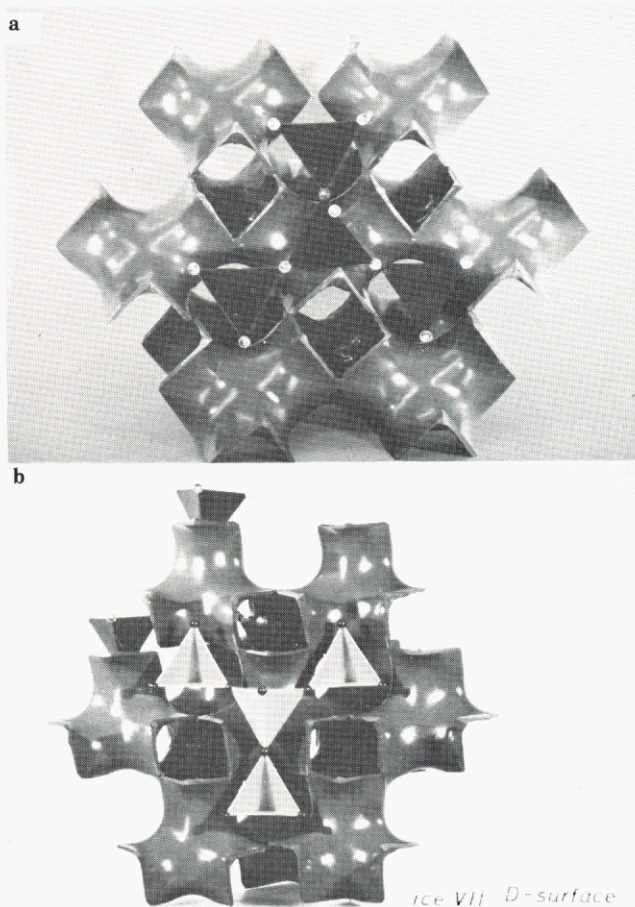

Figure 31. (a) Cubic ice and the F surface. (b) Ice VII and the F surface.
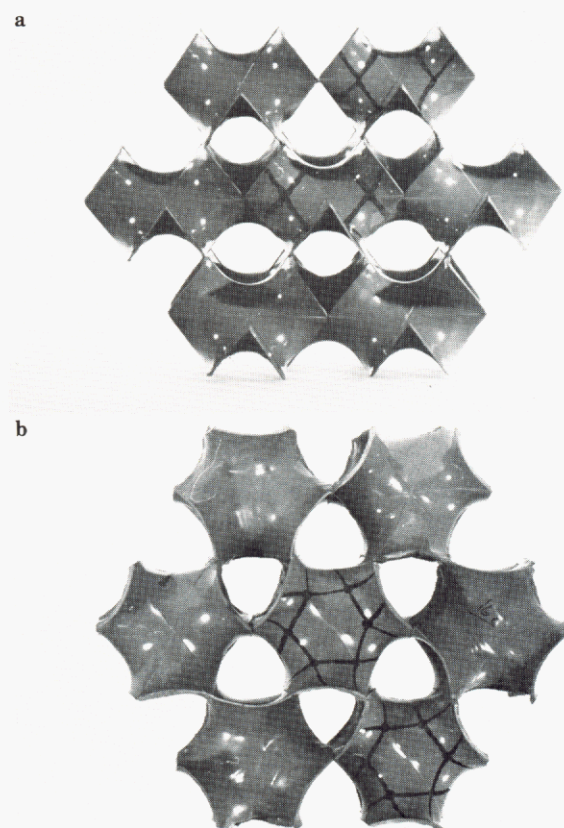

Figure 32. (a) Sodalite structure and the F surface. (b) Analcime structure and the gyroid.
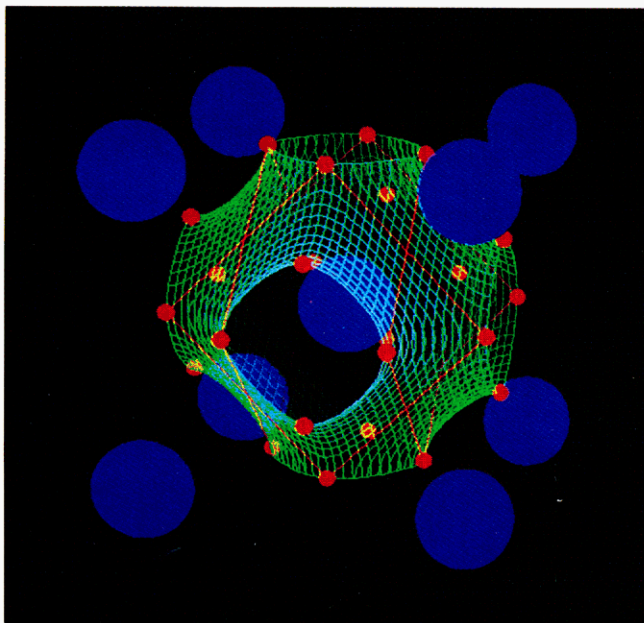
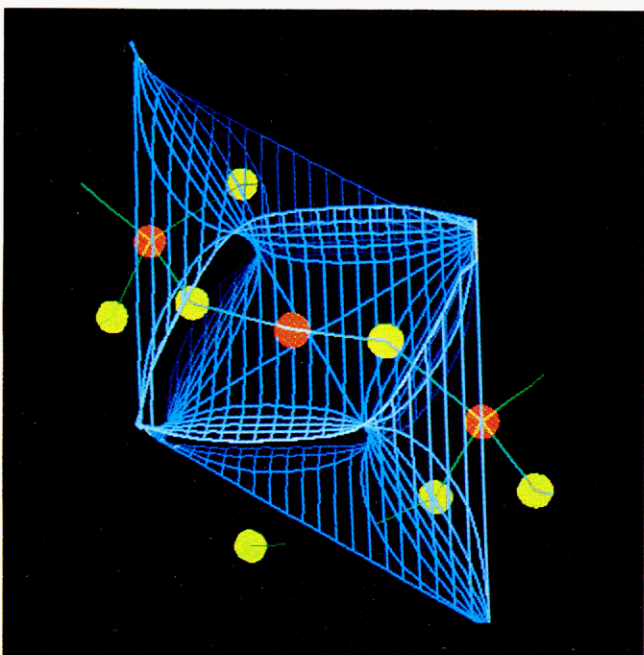**Figure 33.** The ionic conductor AgI and the P surface.

Figure 35. The quartz surface.

Figure 34. The quartz structure and its surface.
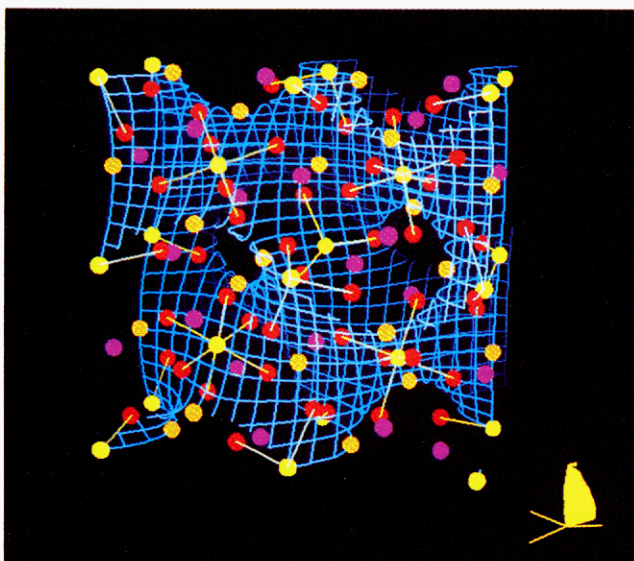
Figure 36. The garnet structure and the gyroid.

terpenetrating and fits on the gyroid surface (Figure 32b). Thus it is easy to imagine a simple translation between the two structures—the surfaces are related by a Bonnet transformation.[2] Another zeolite structure which is noninterpenetrating is hexagonal gmelinite, and a suitable surface is the H surface.[36]

Nesper and von Schnering have investigated PEPS (periodic equipotential surfaces) of Coulombic fields of simple field charges in various space group symmetries.[9,10] They have established that the periodic zero-potential surfaces (POPS) are very similar to the respective periodic minimal surfaces of the same symmetry. They claim that it does not hold that in the case of POPS that the mean curvature is zero; from the interchangeability of (+) and (−) it follows that the *overall* mean curvature disappears ($H = 0$). With von Schnering and Nesper's work we have immediate ex-

amples of the physical applications of periodic minimal surfaces. An elegant example of this is the PEPS for CsCl obtained for the charge distribution (+) on the Wyckoff position 1a and (−) on 1b in $Pm3m$, respectively, that is the Schwartz P surface characterized by $P^{(+)}_{(1a)} \Lambda P^{(-)}_{(1b)}$ with the space group $Im3m$. In the same way the Schwartz D surface is obtained from the combination $D^{(+)}_{(8a)} \Lambda D^{(-)}_{(8b)}$ in $Fd\bar{3}m$. The surface then belongs to the space group $Pn\bar{3}m$, since the generating point configurations already have $Fd3m$ symmetry. Analogously, using the $P622$ symmetry, a POPS was calculated which is useful for the quartz and starch (see below) structures. Nesper and Schnering have also calculated with this Ewald procedure the gyroid surface and have shown how the garnet structure beautifully follows this $Ia3d$ geometry. They have also computed several new surfaces. Figures 33–36 are from their work.

XII. Diffusion in Crystals

The link between electrostatics of a charged lattice and periodic minimal surfaces has been established by the equipotential calculations of Nesper and von Schnering described elsewhere in this article. Two topologically equivalent, (maximally) interpenetrating oppositely charged lattices are conjectured to be separated by a zero equipotential surface which is a periodic minimal surface.

If an ion diffusing within a crystal lattice is assumed to move under the influence of the electrostatic field set up by the lattice, a simple constraint on the trajectory of the diffusing ion is that it follow electrostatic field lines of the lattice. Invariably these field lines form closed orbits about lattice ions; however, under certain conditions, loci of field lines exist which traverse throughout the lattice, forming open orbits. We call the surface supporting these open orbits a "tangential field surface". If an external electric field is applied to a lattice, the existence of an open tangential field surface may result in a net conductivity in the crystal, as in a solid-state electrolyte.

Typical solid electrolytes consist of a crystalline skeletal lattice which is relatively immobile and a disordered array of highly mobile ions, which are responsible for the conductivity of the crystal. Neglecting thermal vibrations of the skeletal lattice, as well as interactions between mobile ions, the conductive paths are expected to lie on tangential field surfaces defined by the skeletal lattice.

It turns out that the tangential field surfaces for lattices are identical with the zero equipotential surfaces for closely related charge arrays, if and only if the equipotential surface is a minimal surface. Rigorously stated, the zero equipotential surface for a charge array of two maximally interpenetrating oppositely charged sublattices is identical with the tangential field surface for the geometrically identical array, with all charges of identical sign. For example, the zero equipotential surface for the cesium chloride structure (the P surface) is a tangential field surface for a body-centered cubic array of like charges. Thus, the problem of determining ionic trajectories in solid electrolytes reduces to determining maximally interpenetrating pairs of sublattices which are equivalent to the skeletal lattice.

We take two examples of this procedure: body-centered and face-centered cubic skeletal lattices. As mentioned above, the P surface is a suitable tangential field surface for the bcc lattice. This lattice can also be decomposed into two maximally interpenetrating diamond sublattices.[44] The zero equipotential for two oppositely charged diamond lattices has been found to be the F surface.[9] Thus, the D surface represents a further tangential field surface for the bcc skeletal lattice. The body-centered symmetry is achieved by interpenetrating two (face-centered) D surfaces, corresponding to the two possible diamond decompositions. This construction yields equivalent saddle polyhedra about each skeletal ion, formed from a skew hexagonal circuit in the D-surface linear skeletal net.

Since a face-centered cubic array corresponds to a body-centered tetragonal array with a c/a ratio of $2^{1/2}:1$, tangential field surfaces for this lattice are generated by tetragonal distortions of the bcc tangential field surfaces. Distortion of the D surface yields the T

surface. In order to form a tangential field surface of cubic symmetry, three mutually orthogonal T surfaces must be interpenetrated. A tetragonally distorted P surface of the required axial ratio is not known.

The classical example of a solid electrolyte is α-AgI, in which the iodine ions form a relatively immobile bcc array and the silver ions are "disordered".[47] Under the simplifying assumptions outlined above, the silver ions are expected to traverse one of the tangential field surfaces derived for the bcc array. Similarly, β-PbF$_2$,[48] and the partially stabilized phase of zirconia, ZrO$_2$, contain fcc skeletal lattices. Thus the fluorine and oxygen anions respectively are expected to follow paths on the T surface.

The validity of this construction is difficult to assess, since little is known experimentally about mobile ion conduction paths. However, available data suggest that the conducting ions do indeed move along periodic minimal surfaces.[49] It is significant that for α-AgI, β-PbF$_2$, and partially stabilized zirconia the measured average positions of the mobile ions lie on tangential field surfaces. A serious shortcoming of the analysis is the neglect of interactions between mobile ions. Inclusion of these interactions could well further support the minimal surface model, given Greenspan's findings discussed elsewhere in this article.

Since the force accelerating mobile ions along the tangential field surface is entirely tangential to the surface (under our assumptions), the curvature component normal to the surface of the ionic trajectories should be zero. In the jargon of differential geometry, we require paths on these surfaces with vanishing normal curvature, so that mobile ions follow asymptotic paths on the tangential field surfaces. The tangential component of the curvature—the geodesic curvature—is expected to be proportional to the magnitude of the field.

This link between forces acting upon a charge and the curvature of the surface confining the charge is widely applicable. For example, an interstitial ion tunneling through a CsCl lattice along the (sterically favored) zero equipotential would be subject everywhere to a force normal to the surface. Consequently, the geodesic curvature of the path of the interstitial must vanish, and it follows lines of curvature on the P surface. For further discussion of these links between curvature and forces, see above.

XIII. The Bonnet Transformation and the Martensite Transition

If austenite (fcc array of iron atoms, with carbon occupying interstitial positions) is cooled slowly, perlite, a mixture of pure iron (α-Fe) and Fe$_3$C, is formed. If cooled very quickly, austenite transforms at relatively low temperature to martensite, which is a tetragonal distortion of the bcc ferrite structure, due to interstitial carbon of the same composition as the parent austenite phase. The bcc structure is sterically unsuitable to contain carbon—martensite is metastable.

Crystallographically the transformation is from fcc to bcc, or bct, in the Fe-C system and is very common among alloys. It can be characterized in the following ways.

1. A structural change involving drastic rearrangements of atoms with no diffusion takes place.
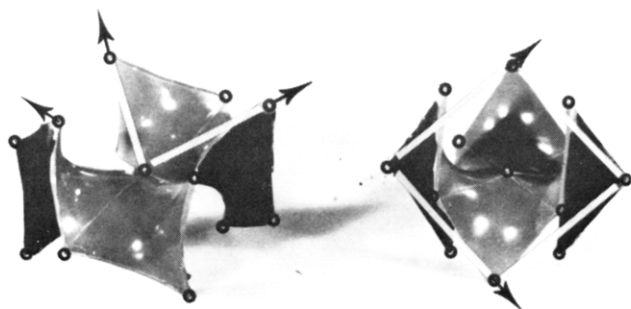
Figure 37. Monkey saddles of the gyroid (left) and the D surface (right). The three cubic lattice vectors of the bcc lattice are shown for the gyroid, and two lattice vectors defining a cube face of the fcc cell are shown for the D surface. All visible flat points are ringed for both saddles.

2. The material undergoes a macroscopic shape change, with sheared blocks in the transformed region. Straight lines inscribed in the surface of the original phase are transformed into connected straight lines in the product, while the characteristic habit plane is essentially undistorted.

3. There exists a precise orientational relationship between the parent and the product phases, with an irrational plane of coexistence of the two phases (the habit plane). The transformed regions are thin plates.

4. The transformation occurs with extremely high velocity, with transformation kinetics independent of temperature over a wide range of temperatures.

5. There is no, or a very small, energy exchange.

The conventionally accepted theories[37,38] utilize matrix algebra in a so-called lattice correspondence theory, derived from the Bain model, which provides a simple topological transformation between the fcc and bcc unit cell. The Bain mechanism involves a compression along one of the cube axes of ~17% and an expansion of ~12% along the other two axes.

These matrix algebra theories require a delicate balance of lattice deformation matrix, shear, and rotation operations to produce the desired results. The theory is essentially a metallurgist's black box, its physical significance being of little importance. The three matrix operations have been developed purely as a mechanism to form physically observed orientations.

A recent comment on the matrix algebraic theories of martensitic transformations indicates the internal lack of physical insight in these theories: "These theories were widely acknowledged due to the excellent agreement between their predictions and the observed features. However, they are unable to describe the physical paths of the atoms during the transformation.... Another difficulty arises for the crystallographic orientation relationships, which are currently deduced from the theory, but without any clear understanding of the physical origin".[39]

We propose here that by using differential geometry, these three algebraic operations can be substituted for one, viz., the bending of a surface to explain the martensite transition. It corresponds to the most restrictive surface transformations of all, viz., the Bonnet transformation, which leaves the Gaussian curvature of the surface at all corresponding points unchanged (see above).

The flat points of the D surface form an fcc lattice, while the flat points of the gyroid form a bcc lattice.
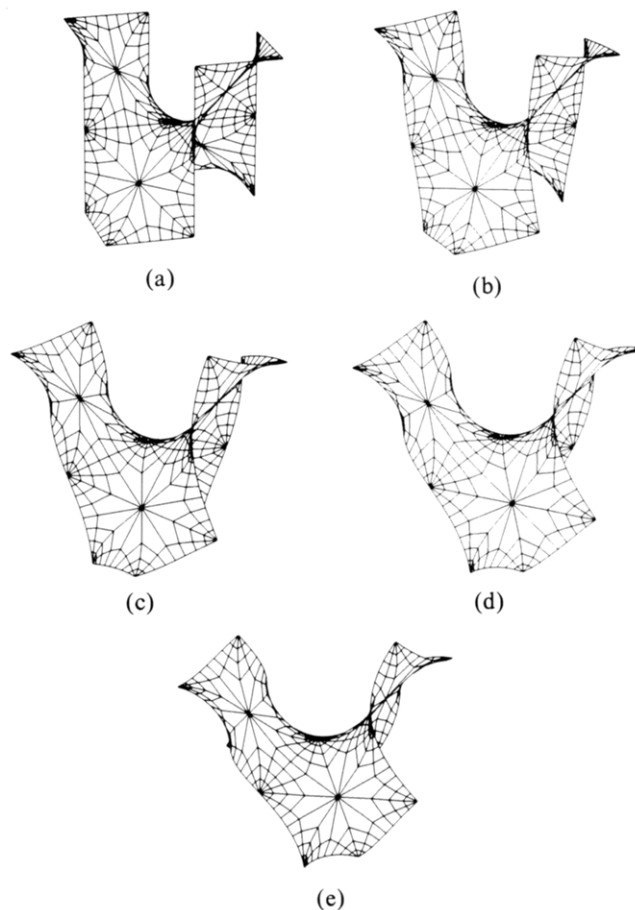

Figure 38. A saddle of the D surface bends to the gyroid via association parameters 0° (a), 10° (b), 20° (c), 30° (d), and 38.015° (e). The flat points of the F surface (a regular tetrahedron) form a fcc lattice, and the corresponding flat points of the gyroid form a bcc lattice.

These lattices are related to each other isometrically by the Bonnet transformation (Figure 37). We propose that the martensite transformation which relates these two phases follows the Bonnet transformation, with all atoms fixed on the transforming surface at flat points, so that all intermediate structures are themselves minimal surfaces.

The isometric nature of the Bonnet transformation fixes the relative dimensions of all associate surfaces. The relative lattice parameters of the martensite phases of iron are uniquely determined by the Bonnet transformation. From the relative dimensions of the tetrahedra in the D surface and the gyroid, the ratio of the lattice parameters for austenite and martensite was determined to be 1.269. Typical data for the two phases are as follows: austenite, 3.591 Å; martensite, 2.875 Å. These parameters give a ratio of 1.249, differing by less than 1% from the value expected from the Bonnet transformation, well within the tetragonal distortion.

Figure 38 shows how a saddle bends from the D surface to the gyroid. The transformation of this simple saddle bends the rectilinear edges into skew curves, with the flat points (iron atoms) tracing out ellipses centered on the midpoint of the saddle (which marks the origin of the transformation), so that the ellipses are increasingly large as we move outward from the origin.

Numerous studies have shown that there is a well-defined orientational relationship between the phases,
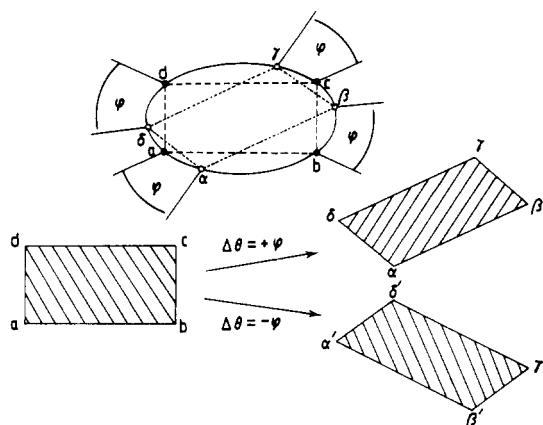
Figure 39. Schematic view of the effect of the Bonnet transformation on a crystal. The elliptical trajectories of all atoms result in a bulk region abcd being transformed into the related sheared and rotated regions $\alpha\beta\gamma\delta$ and $\alpha'\beta'\gamma'\delta'$ for increasing and decreasing association parameter, respectively.

known as the Kurdjomov–Sachs relationship. The plane correspondence is (111) austenite || (011) martensite, and an invariant line has also been repeatedly detected: $[01\bar{1}]$ || $[11\bar{1}]$. The relative orientations of associate surfaces are fixed by the Bonnet constraint that the normal vectors of the surfaces at correponding positions be parallel. There are four possible paths for the Bonnet transformation to proceed: $0° \rightarrow 38.015°$, $0° \rightarrow -38.015°$, $180° \rightarrow 141.985°$, and $180° \rightarrow 218.015°$. The equivalence of all four orientations for the gyroid implies the unique orientational relationship experimentally observed.

The experimentally determined line correspondence is also in agreement with that formed by the Bonnet transformation.

We conclude that the Bain model is a lattice unit cell correspondence for the two phases. The Bonnet model involves correspondence of the largest possible equivalent unit cells in parent and product phases—the entire crystal. All atoms move simultaneously—this crystal correspondence is indeed diffusionless and does not require the large distortions formed in each Bain unit cell according to conventional lattice correspondence matrices. The elliptical orbits of the constituent atoms result in a transformation which may be considered as a shear as well as a rotation as illustrated in Figure 39.

XIV. Biological Significance of Minimal Surfaces

1. Lipid–Water Phases

Due to their amphiphilic character, lipid molecules associate in water into liquid-crystalline phases. The most common is the lamellar liquid-crystalline phase, where lipid bilayers alternate with water layers. A unique feature in the lipid–water structures is the short-range disorder combined with long-range order in one, two, or three dimensions. Thus, on atomic distances, the water molecules and the methylene groups of the hydrocarbon regions are as disordered as in the liquid state. Still there is perfect repetition over long distances. In the lamellar phase, for example, the unit period is equal to the thickness of the lipid bilayer and one adjacent water layer.

The most complex of the lipid–water phases exhibit cubic symmetry. It was recently found that cubic lipid–water phases consist of an infinite lipid bilayer, which in fact is an infinite periodic minimal surface. The existence of these phases has improved our understanding of lipid–water phases in general. The lamellar liquid-crystalline phase can also be described as a minimal surface structure, the extreme case with infinite curvature everywhere. The cubic phases will first be discussed, and then the mechanisms of phase transitions will be described.

The minimal surface structures of lipid–water phases were first revealed in monoglycerides.[51-54] All three basic cubic minimal surfaces, the primitive P, the diamond surface D, and the gyroid G, have now been found, and the structure of one such phase can be seen in Figure 12b. The lipid bilayer center, which is the methyl end group gap, constitutes the minimal surface, with non-Euclidean mirror symmetry relating the two lipid monolayers on each side. The infinite intersection-free lipid bilayer separates the two water channel systems on each side of the lipid bilayer. Conclusive proof of this type of structure was obtained from the existence of two cubic phases within one region of the binary monooleylglycerol–water system. Thus the X-ray dimensions at the transition from the D surface to the diamond surface were in agreement with the theoretical transformation between these two surfaces, the Bonnet transformation.[6] The fact that we could not detect an enthalpy of transition is also consistent with such a mechanism of phase transition.

We have analyzed the phase transitions further in terms of changes in the molecular geometry. It is now generally accepted that changes in molecular wedge shape by temperature or by water–polar head group interaction, as demonstrated by Israelachvili et al.,[50] can fully explain phase transitions in lipid–water systems. Thus a tendency of an increased wedge shape from the polar head toward the methyl end of a lipid molecule is always a result of heating. This provides a driving force toward a phase transition, and one example of such a transition observed experimentally gives the gyroid phase from the lamellar liquid-crystalline phase.[54] The polar head groups are assumed to be located on parallel surfaces on each side of the minimal surface (distance from minimal surface to parallel surface equals the molecular length).

An analysis of the transition in the monoolein–water system from the gyroid surface structure to the D surface with increasing water content (at room temperature and 35.2% (w/w) water) shows that there is an increase in molecular wedge shape from 1.27 to 1.31. If the wedge shape of the molecule is characterized by the molecular volume (V), head group area (a), and tail length (l), the parallel surface construction yields the packing equation

$$\frac{V}{al} = 1 + Hl + \frac{1}{3}K\,l^2$$

where H and K denote the average and Gaussian curvatures of the interface traced out by the head groups. For a bilayer with equivalent lipid composition on both sides of the bilayer, the packing parameter on the left-hand side of the packing equation is equal for ± 1, so that the linear term in l on the right-hand side must vanish. Thus, such a bilayer must be a minimal surface.

While the average curvature is everywhere zero on such a bilayer, the Gaussian curvature varies from point to point along the surface. In order to effectively use the packing equation an average value of the Gaussian curvature is required, in order to give an average molecular shape. This is related to the surface area and topology by

$$\frac{V}{al} = 1 \frac{2\pi}{3A} \chi \ l^2$$

where A denotes the surface area per unit cell of the minimal surface and χ is the Euler characteristic per unit cell.

The transitions lamellar to cubic phases and finally to hexagonal ones can all be understood from changes in wedge shape, either by increased thermal mobility along the hydrocarbon chain or a similar disorder induced by increased water content. Within a cubic phase region of the phase diagram, however, the increased water swelling must result in an increase in unit cell size and thus a decreased curvature of the lipid bilayer. This means that the wedge shape is reduced by water swelling, and a strain is therefore built up in the structure which ultimately results in a phase transition. The transition from the gyroid structure to the D surface curved lipid bilayer discussed above is an illustrative example.

Heating without change in composition has been followed by diffraction pattern versus temperature recordings in the monoglyceride of linoleic acid. There is a lattice shrinkage of about 1% per 2 °C. This means that the bilayer gets thinner and the ratio between the minimal surface and the parallel surface corresponds to an increased molecular wedge shape.

The cubic lipid–water structures described above can accommodate proteins into their structure in two ways. Globular proteins with molecular masses up to 150 000 daltons can be incorporated into the aqueous channel systems,[52] and a considerable increase in lattice dimensions can be obtained in this way. Thus a unit cell axis of 235 Å was observed in a sample of monoolein/lysozyme/water in the weight ratio 31.6:34.2:34.2, and thermal analysis showed a lysozyme transition enthalpy corresponding to water environment.[52]

Strongly amphiphilic proteins exhibiting self-association, however, form minimal surface phases with the proteins partly embedded in the lipid bilayer. Such a phase formed by caseins has been examined by electron microscopy, and the lattice dimensions appear to be extremely large.[53]

In lipid–water systems,[54] as well as in lipid–protein–water systems,[52] cubic phases of all three types of fundamental minimal surfaces have been observed. These cubic phases—P, D, and G—have space groups $Im3m$, $Pn3m$, and $Ia3d$, respectively.[54] The reversed type of structure, formed by an anhydrous lipid, has also been observed[54] (i.e., the center of the polar sheet of the bilayer forms the minimal surface, with hydrocarbon chains filling the channel networks on both sides). Thus there are six alternative cubic structures in which the lipid bilayer is curved according to a fundamental minimal surfaces: P, D, and G, with the lipid bilayer center forming the minimal surface in lipid–water systems, and P^r, D^r, and G^r in anhydrous lipids, where the polar sheet of adjacent bilayers forms the minimal surface.
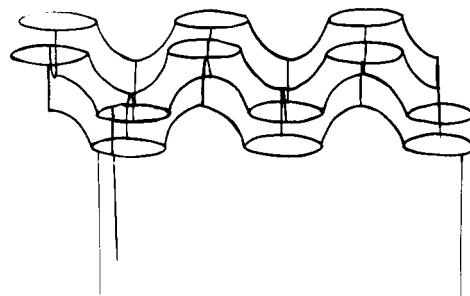

Figure 40. Proposed minimal surface curved lipid bilayer model of membranes.

Besides the lamellar phase, hexagonal phases are most common in lipid–water systems. We have recently analyzed transitions from cubic to hexagonal phases in monoacyl–glycerol–water systems and found evidence indicating that also hexagonal phases are minimal surface structures.

2. Periodic Minimal Surface Curvature of the Lipid Bilayer in Cell Membranes

The present picture of biological membranes involves a lipid bilayer with a structure corresponding to that of the lamellar liquid-crystalline phase. In this traditional model the lipid bilayer has a rather passive role in the different membrane functions. In the earlier paragraph we discussed the unique structural property of lipids in exhibiting long-range order combined with short-range disorder. It would be remarkable if cell membranes did not utilize this feature as well as the ability to undergo phase transitions to switch from one structure to another when there are environmental changes (i.e., a change in pH). The cubic infinite periodic minimal surface structure of the lipid bilayer provides a basis for a new structure model of biomembranes, involving phase transitions between planar and periodically curved bilayers. Evidence supporting this type of membrane structure will be presented below.

We can select planes in the cubic structures P and D discussed above, which give a two-dimensional minimal surface with zero average curvature at all points. We have to cut out such a surface from the adjacent two-dimensional surfaces, giving "holes" upward and downward. Provided that protein molecules can plug these holes, the membrane lipid bilayer can form such an infinite periodic minimal surface. The two simplest surfaces follow the (100) plane of the P phase and the (111) plane of the D phase described above. The P type of structure is shown in Figure 40. These two-dimensional surfaces give a tetragonal or hexagonal arrangement, respectively, of the membrane proteins, provided that proteins plug the "holes" in the surface. Such ordered arrays of proteins have in fact often been observed in membranes.

The possibility of phase transitions involving periodic minimal surface curvature occurring in membranes was recently proposed, and cooperative membrane phenomena were discussed in relation to such transitions.[8a] The differential geometry of such a membrane has been analyzed, including transformations corresponding to continuous variations of the bilayer curvature toward the planar bilayer as an extreme.[8b]
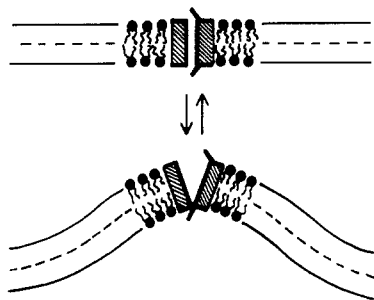
Figure 41. Proposed mechanism of action of general anesthetics. The induced transition planar → curved bilayer results in a blocking of the sodium channel.

General anesthetics are known to act on the lipid bilayer of the neuronal membrane so that the sodium channels are closed, blocking the transmission of the signal propagation. The mechanism behind this effect, however, is not known. There is strong evidence to suggest that the phase transition model presented here can explain the anesthetic effect.[55]

The addition of very low concentrations of inhalation anesthetics such as chloroform, halotane, or ethyl ether was found to result in a phase transition in aqueous liposomal dispersions of phosphatidylcholines (from egg yolk and soybeans) from the lamellar liquid-crystalline structure into the cubic phase, with minimal surface curved bilayers. It is probable that such a change in curvature of the lipid bilayer of the axon membrane will induce a conformational change in the sodium channels. The proposed mechanism is shown in Figure 41. The pressure antagonism of the anesthetic effect can be directly explained by this model. An increase in pressure will always give a phase transition opposite to the one induced by anesthetics, provided the pressure of transition is reached.

Formation of so-called lipidic particles in model membranes is considered to play a role in membrane fusion.[56,57] It is quite obvious that the three-dimensionally arranged lipid bilayers of the minimal surface cubic structures are ideal in providing the functions postulated for lipidic particles, such as fusion and trans-bilayer transport properties. Freeze–fracture electron micrographs of the lipidic particles[56] often show similar textures as those of the cubic minimal surface structure.[58] Also in a paper on the structural role of lipids in the photosynthetic membrane, which is based on electron microscopy studies of corresponding lipid dispersions,[59] electron micrographs with the same appearance as the cubic phase are shown (assumed to be close-packed arrays of inverted micelles in lipid bilayers).

Luzzati and co-workers have recently studied the phase properties of lipids from *S. solfataricus* membranes, and on this basis a membrane model has been proposed[60] which is equivalent a periodically curved bilayer with protein "plugs".

The prolamellar body, which is a three-dimensional storage form of thylakoid membranes, shows morphologies in electron microscopy like a cubic minimal surface structure. The ultrastructure has been derived by Gunning,[61] and it is in fact consistent with a minimal surface with space group *Im3m*. Helfrich and co-workers[62] have observed "passages" between egg lecithin bilayers with a primitive cubic symmetry (*Pm3m*). The

same type of structure has been described at the regions of fusion of liposomes by Glad et al.[63] A double-membrane system has been observed in the luminal surface of the intestinal wall from an insect.[64] The ultrastructure corresponds to two fused bilayers of a cubic minimal surface structure.

The exchange of the plasma membrane bilayer by endocystosis has been quantified in numerous studies, showing that the average residence time for membrane material on the cell surface is about half an hour. Furthermore, the cell surface area excess is about threefold in relation to the area of the corresponding smooth sphere. The periodically curved bilayer model presented here provides possibilities for direct control mechanisms of membrane bilayer dynamics. Thus the curved bilayer is able to accommodate varying amounts of lipid bilayer per unit front of membrane.[8a] An endocystosis model based on such a lipid bilayer phase transition, controlled by specific structural parameters, is discussed below.

On the basis of our knowledge of lipid bilayer phase transitions, we postulate that the average molecular wedge shape and the hydrostatic pressure gradient over the membrane determine the average curvature and periodicity of homogeneous membrane regions. The relation between average curvature and the pressure gradient over the membrane is given by the Laplace–Young equation. It should be pointed out that a constant average curvature different from zero must be common in order to account for pressure gradients. The successive change of the curvature of the ER system (planar rough ER region to curved smooth ER) toward formation of spherical vesicles furthest out might be controlled in this way. The endocystosis process can in fact also be "curvature controlled", once the actual particle has reached the receptor. Applying the relations between adsorption and Gaussian curvature demonstrated above, it is obvious that the increase in interaction between particle and membrane can be the driving force for the budding out process to the final cutoff of a vesicle. An alternative to clathrin monitoring the endocystosis process which should be considered is a bilayer curvature control, with the clathrin network acting as a skeleton quantizing the curvature.

The beauty of the periodically curved lipid bilayer model is that it provides organization and control of membrane phenomena that otherwise seem to occur rather arbitrarily in time and space, for example, the requirement of rapid mass fusion of synaptic vesicles with the presynaptic membrane in connection with transmission of the nerve impulse. A phase transition of this membrane involving a periodically curved bilayer would give the cooperativity needed in this process (and the opposite transition can account for recycling of the bilayer material).

3. Biopolymers

The double-helix structure, which can be described as a minimal surface, is a common feature in many biopolymers, for example, the actin/myosin complex and DNA. We will discuss another such structure here, that of native starch. Minimal surface concepts make a complete description of the molecular organization in starch granules possible.[7]

Figure 42. Molecular model of the α,1–6 linkage between double helices. The distance between helical axes (the a axis) is about 20 Å, and the pitch is also about 20 Å.

The branched polyglucan amylopectin, constituting about three-fourths of the starch granule, is mainly crystalline,[65] whereas the linear polymer amylose is amorphous, acting as a space filler. The amylopectin molecule is one of the largest known in nature, and its branching organization has recently been determined.[66] The branches form clusters, with chains radially distributed from the reducing end of the molecule and the clusters according to EM studies[67] packed in concentric crystalline layers in the granule. The diameter of the cluster is about 100–150 Å and the thickness is about 50 Å.

From the X-ray diffraction pattern the close-packing arrangement of glucan chains in the crystalline regions has been determined.[68] The chains form double helices, which are hexagonally packed. In tuber starch compared to cereal starch every sixth double helix is replaced by water, and in the continuing discussion we will consider the cereal starch structure.

By molecular modeling it was shown that the geometry of branching, the α,1–6 glucoside linkage, fits into the van der Waals packing of double helices, as shown in Figure 42. This is one of the most remarkable properties of the starch structure and explains how branching points on polyglucan can phase separate into crystalline units.

A striking agreement between the structure of quartz and that of starch was detected. Quartz (high quartz with right-handed SiO_4 helices) can be described by a self-intersecting minimal surface with space group $P6_422$ (the unit cell of starch is slightly deformed). Common features are the arrangement of six SiO_4 tetrahedra or glucose units, respectively, as structural units and the
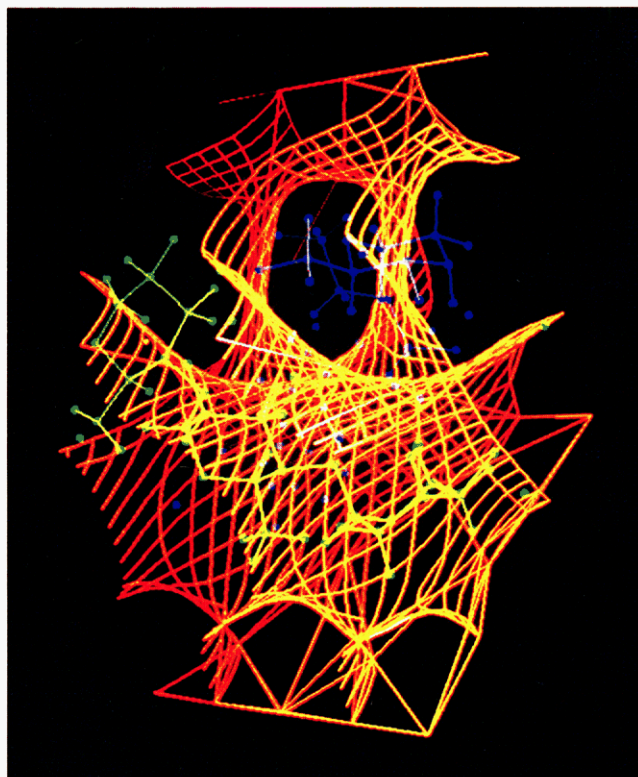

Figure 43. Part of the quartz surface, intersecting along the c axis, with the polyglucan double helix superimposed.
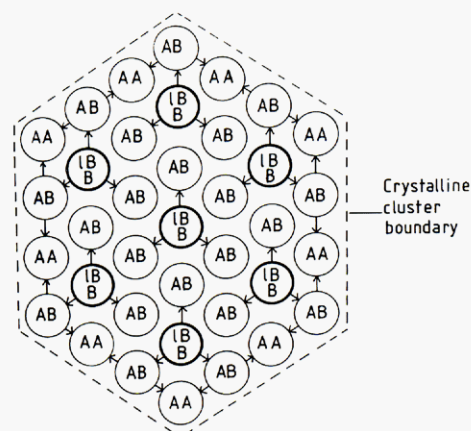

Figure 44. Packing of the double helices (seen along their axes) in a crystalline amylopectin cluster. Arrows indicate branching points. B chains are polyglucan chains which in turn are branched, whereas A chains are final branches. A long B chain, lB, comes from the cluster below.
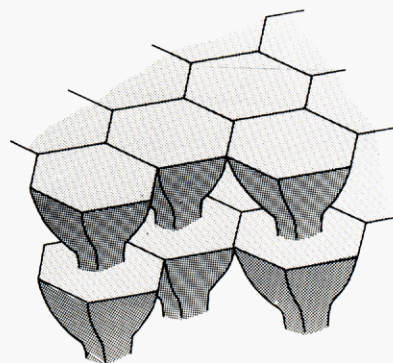

Figure 45. Cluster arrangement in the concentric layers of the starch granule.

distance between adjacent double helices, corresponding to the branching geometry (reflected in the similarity in the a/c ratio). A description of the amylopectin crystalline packing and the relation to the minimal surface of quartz are given in Figure 43.

The branching pattern of a crystalline cluster was also analyzed, and only one system of branching was found to be consistent with the configurations of α,1,6 linkages derived from enzymatic degradation. A cross section of a cluster is shown in Figure 44.

The overall structure of the crystalline units of the starch granule is illustrated in Figure 45. Between each cluster (with cross section shown in Figure 44) amylose in amorphous form fills the empty space. This structure gives a deeper understanding of many properties of starch, such as gelatinization and retrogradation.[7]

References

(1) Andersson, S.; Hyde, S. T.; von Schnering, H. G. *Z. Kristallogr.* **1984**, *168*, 1.
(2) Hyde, S. T.; Andersson, S. *Z. Kristallogr.* **1984**, *168*, 221.
(3) Hyde, S. T.; Andersson, S. *Z. Kristallogr.* **1985**, *170*, 225.
(4) Hyde, S. T.; Andersson, S. *Z. Kristallogr.* **1986**, *174*, 225.
(5) Thomasson, R.; Lidin, S.; Andersson, S., in press.
(6) Hyde, S. T.; Andersson, S.; Ericsson, B.; Larsson, K. *Z. Kristallogr.* **1984**, *168*, 213.
(7) Eliasson, A.-C.; Larsson, K.; Andersson, S.; Hyde, S. T.; Nesper, R.; von Schnering, H. G. *Starke*, in press.
(8) (a) Hyde, S. T.; Andersson, S.; Larsson, K. *Z. Kristallogr.* **1986**, *174*, 237. (b) Larsson, K.; Andersson, S. *Acta Chem. Scand., Ser. B* **1986**, *B40*, 1.
(9) Nesper, R.; von Schnering, H. G. *Z. Kristallogr.* **1985**, *170*, 138.
(10) (a) Nesper, R.; von Schnering, H. G. *Angew. Chem.* **1986**, *98*, 111. (b) von Schnering, H. G. *Z. Kristallogr.* **1986**, *174*, 182.
(11) (a) Hyde, S. T., to be published. (b) Lidin, S.; Hyde, S. T. *J. Phys. (Les Ulis, Fr.)*, in press.
(12) Hyde, S. T., to be published.
(13) Fischer, W.; Koch, E. *Z. Kristallogr.*, in press.
(14) Schwarz, H. A. *Gesammelte Mathematische Abhandlungen*; Springer: Berlin, 1890.
(15) Neovius, E. R. *Bestimmung Zweier Spezieller Periodische Minimalflächen*; J. C. Frenckel & Sohn: Helsinki, 1883.
(16) Shoen, A. H. *NASA Tech. Rep. No. 05541*, 1970.
(17) Donnay, G.; Pawson, D. L. *Science (Washington, D.C.)* **1969**, *166*, 1147.
(18) Nissen, H. U. *Science (Washington, D.C.)* **1969**, *166*, 1150.
(19) Scriven, L. E. *Nature (London)* **1976**, *266*, 123.
(20) Larsson, K.; Fontell, K.; Krogh, N. *Chem. Phys. Lipids* **1980**, *27*, 321.
(21) Mackay, A. IUC Copenhagen Meeting, Poster, 1979.
(22) Hyde, B. G.; Andersson, S.; Bakker, M.; Plug, C.; O'Keeffe, M. *Prog. Solid State Chem.* **1978**, *12*, 273.
(23) Andersson, S.; Hyde, B. G. *Z. Kristallogr.* **1982**, *168*, 119.
(24) Yang, Q. B.; Andersson, S. *Acta Crystallogr., Sect. B* **1987**, *B43*, 1.
(25) Gordon, E. K.; Samson, S.; Kamb, W. B. *Science (Washington, D.C.)* **1966**, *154*, 1004.
(26) Andersson, S.; Fälth, L. *J. Solid State Chem.* **1983**, *46*, 256.
(27) Fischer, W.; Koch, E. *Acta Crystallogr., Sect. A* **1976**, *A32*, 225.
(28) Fälth, L.; Andersson, S. *Z. Kristallogr.* **1983**, *160*, 313.
(29) Andersson, S. *Angew. Chem., Int. Ed. Engl.* **1983**, *22*, 69.

(30) Nagano, T.; Smyth, B. *Commun. Math. Helvet.* **1978**, *53*, 52.
(31) Goursat, E. *Acta Crystallogr.* **1888**, *11*, 135.
(32) Thomasson, R.; Lidin, S.; Andersson, S. *Angew. Chem.*, in press.
(33) (a) Stach, H.; Lohse, U.; Tamm, H.; Schirmar, W. *Zeolites* **1986**, *6*, 74. (b) Blum, Z.; Lidin, S.; Andersson, S., to be published.
(34) Louie, A. H.; Somorjai, R. L. *J. Theor. Biol.* **1982**, *98*, 189–209.
(35) Christensen, N. E. *Phys. Rev. B* **1985**, *32*, 207.
(36) Lidin, S., to be published.
(37) Bowles, J. S.; Mackenzie, J. K. *Acta Metall.* **1954**, *2*, 129, 138.
(38) Wechsler, M. S.; Lieberman, D. S.; Read, T. A. *Trans. AJME* **1953**, *197*, 1503.
(39) Gobin, P. F.; Guenin, G. In *Solid State Transformations in Metals and Alloys. Les Editions de Physique*, 1978, p 573.
(40) Coxeter, H. S. M. *Regular Polytopes*, 2nd ed.; Macmillan: New York, 1963.
(41) Schoen, A. Patent Application Abstract, NASA Case No. ERC-10 363.
(42) Bashkirov, N. M. *Sov. Phys.—Crystallogr. (Engl. Transl.)* **1959**, *4*, 442–447.
(43) Smyth, B. *Invent. Math.* **1984**, *76*, 411–420.
(44) Wells, A. F. *Three Dimensional Nets and Polyhedra*; Wiley: New York, 1977.
(45) Greenspan, D. *Appl. Math. Models* **1983**, *7*, 423–426.
(46) Pearce, P. *Structure in Nature Is a Strategy for Design*; MIT Press: Cambridge, MA, 1978.
(47) Funke, K. *Prog. Solid State Chem.* **1976**, *11*, 345–402.
(48) Derrington, C. E.; O'Keeffe, M. *Nature (London) Phys. Sci.* **1973**, *246*, 44.
(49) Andersson, S.; Hyde, S. T.; Bovin, J. O. *Z. Kristallogr.* **1985**, *173*, 97.
(50) Israelachvili, J. N.; Mitchell, D. J.; Ninham, B. W. *J. Chem. Soc., Faraday Trans. 2* **1976**, *72*, 1525.
(51) Lindblom, G.; Larsson, K.; Johansson, L.; Fontell, K.; Forsén, S. *J. Am. Chem. Soc.* **1979**, *101*, 5465.
(52) Ericsson, B.; Larsson, K.; Fontell, K.; *Biochim. Biophys. Acta* **1983**, *729*, 23.
(53) Buchheim, W.; Larsson, K. *J. Colloid Interface Sci.*, in press.
(54) Larsson, K. *J. Colloid Interface Sci.* **1986**, *113*, 299.
(55) Larsson, K. *Acta Chem. Scand., Ser. A* **1986**, *A40*, 313.
(56) Verklei, A. J. *Biochim. Biophys. Acta* **1984**, *779*, 43.
(57) Verklei, A. J.; Mombers, C.; Gerritsen, W. J.; Lennissen-Bijrelt, K.; Cullis, P. R. *Biochim. Biophys. Acta* **1979**, *559*, 358.
(58) Gulik-Krzywicki, T.; Aggerbeck, L. P.; Larsson, K. *Surfactants in Solution*; Mittal, K. L.; Lindman, B., Plenum: New York, 1984; Vol. 1, p 237.
(59) Quinn, P. J.; Williams, W. P. *Biochim. Biophys. Acta* **1983**, *737*, 223.
(60) Luzzati, V.; Gulik, A. *System. Appl. Microbiol.*, in press.
(61) Gunning, B. E. S. *Protoplasma* **1965**, *60*, 111.
(62) Harbich, W.; Servuss, R. M.; Helfrich, W. *Naturforsch., A* **1978**, *33a*, 1013.
(63) Glad, A. E.; Bruza, R.; Eytan, G. D. *Biochim. Biophys. Acta* **1979**, *556*, 181.
(64) Lane, N. J.; Harrison, J. B. *J. Cell Biol.* **1979**, *63*, 271.
(65) Gidley, M. J.; Bociek, S. M. *J. Am. Chem. Soc.* **1985**, *107*, 7040.
(66) Manners, D. J. *Cereal Foods World* **1985**, *30*, 461.
(67) Yamaguchi, M.; Kainuma, K.; French, D. *J. Ultrastruct. Res.* **1979**, *69*, 249.
(68) Wu, H.-C. H.; Sarko, A. *Carbohydr. Res.* **1978**, *61*, 7, 27.
(69) Lidin, S.; Andersson, S., to be published.
(70) Goetz, A. *Introduction to Differential Geometry*; Addison-Wesley: Reading, MA, 1970.
(71) Do Carmo, M. P. *Differential Geometry of Curves and Surfaces*; Prentice-Hall: Englewood Cliffs, NJ, 1976.
(72) Nitche, J. C. C. *Vorelesungen über Minimalflächen*; Springer-Verlag: Berlin, Heidelberg, 1975.
(73) Hildebrandt, S.; Tromba, A. *Mathematics and Optimal Form*; Freeman: New York, 1984.